Unified *ab initio* description of Fröhlich electron-phonon interactions in two-dimensional and three-dimensional materials

Weng Hong Sio [1,2] and Feliciano Giustino [2,3,*]

[1]*Institute of Applied Physics and Materials Engineering, University of Macau, Macao SAR 999078, People's Republic of China*
[2]*Oden Institute for Computational Engineering and Sciences, The University of Texas at Austin, Austin, Texas 78712, USA*
[3]*Department of Physics, The University of Texas at Austin, Austin, Texas 78712, USA*

Ab initio calculations of electron-phonon interactions including the polar Fröhlich coupling have advanced considerably in recent years. The Fröhlich electron-phonon matrix element is by now well understood in the case of bulk three-dimensional (3D) materials. In the case of two-dimensional (2D) materials, the standard procedure to include Fröhlich coupling is to employ Coulomb truncation, so as to eliminate artificial interactions between periodic images of the 2D layer. While these techniques are well established, the transition of the Fröhlich coupling from three to two dimensions has not been investigated. Furthermore, it remains unclear what error one makes when describing 2D systems using the standard bulk formalism in a periodic supercell geometry. Here we generalize previous work on the *ab initio* Fröhlich electron-phonon matrix element in bulk materials by investigating the electrostatic potential of atomic dipoles in a periodic supercell consisting of a 2D material and a continuum dielectric slab. We obtain a unified expression for the matrix element, which reduces to the existing formulas for three-dimensional and 2D systems when the interlayer separation tends to zero or infinity, respectively. This expression enables an accurate description of the Fröhlich matrix element in 2D systems without resorting to Coulomb truncation. We validate our approach by direct *ab initio* density-functional perturbation theory calculations for monolayer BN and MoS_2, and we provide a simple expression for the 2D Fröhlich matrix element that can be used in model Hamiltonian approaches. The formalism outlined in this work may find applications in calculations of polarons, quasiparticle renormalization, transport coefficients, and superconductivity, in 2D and quasi-2D materials.

I. INTRODUCTION

The electron-phonon interaction (EPI) plays an important role in many materials properties [1], including the carrier mobility of semiconductors [2,3], phonon-assisted optical processes [4–6], vibrational spectroscopy [7–9], polaron physics [10–13], and superconducting pairing [14,15]. During the past decade, calculations of EPIs have become more accessible, and much work has been performed on the role of phonons in the optical and transport properties of semiconductors and other functional materials [16–22]. Given the significant interest in two-dimensional (2D) materials and their applications [23–25], *ab initio* calculations of EPIs in 2D systems are also becoming increasingly popular [26–30].

The key element of *ab initio* calculations of EPIs is the electron-phonon matrix element, $g_{mn\nu}(\mathbf{k}, \mathbf{q})$, which describes the probability amplitude for an electron to be scattered from an initial Bloch state with wave vector $\mathbf{k}$ and band index n to a final state with wavevector $\mathbf{k} + \mathbf{q}$ and band index m by a phonon of wave vector $\mathbf{q}$ and branch index ν. In the majority of known three-dimensional (3D) semiconductors and insulators, this matrix element diverges as $1/|\mathbf{q}|$ for small

$\mathbf{q}$, as a result of the long-range nature of the electric field generated by fluctuating atomic dipoles. This singular behavior is referred to as the Fröhlich electron-phonon coupling [31] and occurs whenever the atoms in a crystal exhibit nonvanishing Born effective charges [32–34].

Calculations of EPIs in bulk 3D systems including the Fröhlich coupling are well established by now [32,33] and are routinely performed in conjunction with Wannier-Fourier interpolation [35,36]. In the case of 2D materials, several proposals have been put forward for dealing with the Fröhlich EPI, including parametrized model matrix elements [27,37], calculations using the formalism for 3D systems [30], and fully *ab initio* approaches employing Coulomb truncation [28,29]. All these approaches focus on the case of a monolayer system embedded in a vacuum buffer in periodic supercell calculations. More complex configurations, including van der Waals heterostructures, semiconductor/insulator interfaces, and moiré bilayers [38–41], are still beyond the reach of current methods. Furthermore, the connection between current approaches for 2D systems and the previous theory for 3D systems remains unclear. In order to enable the study of EPIs in a broader class of materials and their interfaces, it is desirable to develop a single unified framework for describing Fröhlich EPIs in 3D and 2D systems on the same footing.

At a more fundamental level, there is also the question on how to connect *ab initio* calculations of EPIs in 2D systems

*fgiustino@oden.utexas.edu

with model Hamiltonian approaches. Earlier work considered the so-called "strict 2D limit" of the Fröhlich matrix element, whereby electrons are assumed to be confined in a sheet of vanishing thickness [42,43]. This limit was successfully employed to investigate polarons and quasiparticle renormalization in 2D systems [44–48], but in this model the matrix element diverges as $|\mathbf{q}|^{-1/2}$ at small $\mathbf{q}$. This behavior contrasts with the fact that, in realistic systems with small but finite thickness, the long-wavelength limit of the Fröhlich matrix elements is finite [49]. This inconsistency poses a challenge when attempting to relate the results derived from earlier models and even recent diagrammatic Monte Carlo studies [48] to atomic-scale *ab initio* calculations of EPIs.

Here we address these difficulties by developing a unified Fröhlich EPI matrix element which seamlessly describes 3D and 2D systems within a periodic supercell geometry. The present approach is a generalization of the approach of Ref. [32] for bulk 3D systems. While Ref. [32] derived the Fröhlich matrix element by examining the electrostatics of a dipole in a bulk crystal, here we examine the potential generated by a dipole within a 2D slab embedded in a uniform dielectric medium (such as vacuum, for example).

We validate this approach by comparing our analytical expressions with explicit density-functional perturbation theory (DFPT) calculations for monolayer BN and MoS$_2$, and we show that our method reproduces the expressions of Ref. [32–34] in the 3D limit, as well as the expression of Ref. [26] in the limit of large interlayer separation between the periodic images of the 2D layer.

The paper is organized as follows. In Sec. II we discuss the formalism to describe Fröhlich EPIs in bulk and 2D materials. In particular, in Sec. II A we review the basics of Fröhlich coupling in bulk 3D materials from the point of view of *ab initio* calculations, and the connection between the *ab initio* formalism and the analytical model originally derived by Fröhlich. In Sec. II B we briefly summarize existing approaches to Fröhlich coupling in 2D systems, the underlying assumptions, and their limitations. In Sec. III we derive an expression for the *ab initio* Fröhlich matrix element in 2D and quasi-2D systems. In Sec. IV we show how our expression recovers the 3D matrix element of Refs. [32–34] (Sec. IV A) and the 2D matrix element of Ref. [26] (Sec. IV B) in the respective limits. In the same section we also derive an expression for the special case of atomically thin single-layer crystals in vacuum, where all the atoms lie in the same plane (Sec. IV C). In Sec. V we rewrite our main results from Sec. IV in a form that depends on only macroscopic quantities and that is particularly suitable for use in model Hamiltonian approaches. Section VI reports applications of this methodology to monolayer BN and MoS$_2$. In particular, in Sec. VI A we provide details on the computational setup and the optimized material parameters. In Sec. VI B we calculate the *ab initio* Fröhlich matrix elements in monolayer BN and monolayer MoS$_2$ and validate our method by direct comparison with DFPT calculations. In Sec. VI C we examine the dependence of the polar coupling on the size of the vacuum gap using our closed-form expressions and *ab initio* materials parameters for BN. In Sec. VII we summarize our findings and offer our conclusions.

II. THE FRÖHLICH ELECTRON-PHONON MATRIX ELEMENT IN 3D AND 2D SYSTEMS: EARLIER WORK

A. Fröhlich coupling in bulk 3D solids

In this section we first recall the expression for the 3D Fröhlich matrix element as derived in Ref. [32]. The same expression was obtained in Refs. [33,34] following a different route. Then we clarify the connection between the *ab initio* Fröhlich matrix element and the classic result by Fröhlich.

The EPI matrix element can be written [1] as $g_{mn\nu}(\mathbf{k}, \mathbf{q}) = \langle \psi_{m\mathbf{k}+\mathbf{q}} | \Delta_{\mathbf{q}\nu} V | \psi_{n\mathbf{k}} \rangle$, where $\psi_{n\mathbf{k}}$ and $\psi_{m\mathbf{k}+\mathbf{q}}$ are typically Kohn-Sham wave functions, and $\Delta_{\mathbf{q}\nu} V$ is the linear variation of the Kohn-Sham potential associated with a phonon of frequency $\omega_{\mathbf{q}\nu}$. $\Delta_{\mathbf{q}\nu} V$ can be calculated using DFPT [50] or the frozen phonon method [51].

Reference [34] showed that, in crystals with a finite gap between occupied and unoccupied states, the EPI matrix element can be expanded in a Laurent series near $\mathbf{q} = 0$. This series may contain terms that scale as $O(q^{-1})$, $O(q^0)$, $O(q^1)$, and so on, where $q = |\mathbf{q}|$. The $O(q^{-1})$ term corresponds to an electric dipole potential, the $O(q^0)$ term corresponds to a quadrupole, the term $O(q)$ is for an octopole, and so on. In materials with nonzero Born effective charges, such as for example polar semiconductors and oxides, the dipole term is nonzero and dominates in the limit $q \to 0$. Since the dipole and quadrupole terms are nonanalytic near $q = 0$, these terms must be treated separately when performing Wannier interpolation of the EPI matrix elements. The *ab initio* procedure to deal with the dipole term was developed in Refs. [32,33], and the corresponding procedure for dealing with the quadrupole term was reported recently in Refs. [52–55]. In all cases one writes the matrix element as

$$g_{mn\nu}(\mathbf{k}, \mathbf{q}) = g_{mn\nu}^{\mathcal{S}}(\mathbf{k}, \mathbf{q}) + g_{mn\nu}^{\mathcal{L}}(\mathbf{k}, \mathbf{q}), \tag{1}$$

where the superscripts stand for short- and long-range, respectively. $g_{mn\nu}^{\mathcal{L}}(\mathbf{k}, \mathbf{q})$ contains all nonanalyticities and is designed to capture the exact limit of $g_{mn\nu}(\mathbf{k}, \mathbf{q})$ for $\mathbf{q} \to 0$. The form of $g_{mn\nu}^{\mathcal{L}}(\mathbf{k}, \mathbf{q})$ away from $\mathbf{q} = 0$ is inconsequential, as long as it is a smooth function of the phonon wave vector.

In the following we focus on the $O(q^{-1})$ component of $g_{mn\nu}^{\mathcal{L}}(\mathbf{k}, \mathbf{q})$, which is commonly known as the Fröhlich interaction. The extension of the present formalism to deal with quadrupoles is possible, at least in principle, but this would require a separate investigation. For notational simplicity, below we drop the superscript in $g_{mn\nu}^{\mathcal{L}}(\mathbf{k}, \mathbf{q})$, and we use $g_{mn\nu}(\mathbf{k}, \mathbf{q})$ to indicate the Fröhlich component of the matrix element.

To obtain the Fröhlich matrix element, Ref. [32] proceeded in two steps: (1) evaluate the electrostatic potential generated by a point dipole $\mathbf{p}$ in an anisotropic medium characterized by the high-frequency relative dielectric permittivity tensor $\boldsymbol{\epsilon}^\infty$ and (2) associate one such dipole to every atom κ in the unit cell with lattice vector $\mathbf{R}$, undergoing the displacement

$$\Delta \boldsymbol{\tau}_{\kappa\mathbf{R}}^{(\mathbf{q}\nu)} = (\hbar/2M_\kappa \omega_{\mathbf{q}\nu})^{\frac{1}{2}} e^{i\mathbf{q}\cdot\mathbf{R}} \mathbf{e}_{\kappa\nu}(\mathbf{q}). \tag{2}$$

Here M_κ is the atomic mass and $\mathbf{e}_{\kappa\nu}(\mathbf{q})$ is the vibrational eigenvector normalized in the unit cell. This atom carries the (dimensionless) Born effective charge tensor $\mathbf{Z}_\kappa^*$. The resulting

matrix element is [32,56]

$$g_{mn\nu}(\mathbf{k}, \mathbf{q}) = i\frac{4\pi}{\Omega}\frac{e^2}{4\pi\varepsilon_0}\sum_\kappa\left(\frac{\hbar}{2M_\kappa\omega_{\mathbf{q}\nu}}\right)^{\frac{1}{2}}$$

$$\times \sum_{\mathbf{G}\neq-\mathbf{q}}\frac{(\mathbf{q}+\mathbf{G})\cdot\mathbf{Z}_\kappa^*\cdot\mathbf{e}_{\kappa\nu}(\mathbf{q})}{(\mathbf{q}+\mathbf{G})\cdot\boldsymbol{\epsilon}^\infty\cdot(\mathbf{q}+\mathbf{G})}$$

$$\times \langle\psi_{m\mathbf{k}+\mathbf{q}}|e^{i(\mathbf{q}+\mathbf{G})\cdot(\mathbf{r}-\boldsymbol{\tau}_\kappa)}|\psi_{n\mathbf{k}}\rangle, \qquad (3)$$

where Ω is the volume of the primitive unit cell, and $\boldsymbol{\tau}_\kappa$ is the equilibrium position of this atom. $\mathbf{G}$ denotes the reciprocal lattice vectors, and the braket indicates the integral over the Born–von Kármán (BvK) supercell.

The classic matrix element by Fröhlich can be obtained from Eq. (3) by considering the following approximations. (1) We consider $\mathbf{q}$ in the first Brillouin zone, so that the only singularity is at $\mathbf{q} = 0$ and the summation over $\mathbf{G}$ can be ignored. (2) For all quantities that vary smoothly with $\mathbf{q}$, we retain only the corresponding $\mathbf{q} = 0$ limit. (3) The band structure is described using the electron gas model, so that $\psi_{n\mathbf{k}}(\mathbf{r}) = (N\Omega)^{-1/2}e^{i\mathbf{k}\cdot\mathbf{r}}$. (4) Phonons are described using the Einstein model, therefore there are two transverse optical (TO) branches with $\omega_{\mathbf{q}\nu} = \omega_{\mathrm{TO}}$ and one LO branch with $\omega_{\mathbf{q}\nu} = \omega_{\mathrm{LO}}$. (v) The dielectric permittivity tensor is isotropic, $\epsilon_{\alpha\beta}^\infty = \epsilon^\infty\delta_{\alpha\beta}$, with Greek indices denoting Cartesian coordinates. Using these approximations in Eq. (3), we find

$$|g_\nu(\mathbf{q})|^2 = \left(\frac{4\pi}{\Omega}\frac{e^2}{4\pi\varepsilon_0}\frac{1}{\epsilon^\infty}\right)^2\frac{\hbar}{2M_0\omega_{\mathrm{LO}}}\frac{|\mathbf{q}\cdot\mathbf{Z}_\nu^*|^2}{q^4}, \qquad (4)$$

where we removed the redundant band indices and we introduced the mode-effective Born charge $\mathbf{Z}_\nu^*$ following Ref. [57], $Z_{\nu,\alpha}^* = \sum_{\kappa,\beta}(M_0/M_\kappa)^{1/2}Z_{\kappa,\alpha\beta}^*e_{\kappa\beta,\nu}(0)$. In these expressions, M_0 is an arbitrary reference mass that is introduced to keep $Z_{\nu a}^*$ dimensionless. The matrix element in Eq. (4) depends on the angle between $\mathbf{q}$ and $\mathbf{Z}_\nu^*$. By performing a spherical average over this angle (taking into account the volume element in three dimensions), and summing over the LO/TO manifold, we obtain a single effective matrix element:

$$|g(q)|^2 = \left(\frac{4\pi}{\Omega}\frac{e^2}{4\pi\varepsilon_0}\frac{1}{\epsilon^\infty}\right)^2\frac{\hbar}{2M_0\omega_{\mathrm{LO}}}\frac{1}{q^2}\sum_\nu|\mathbf{Z}_\nu^*|^2. \quad (5)$$

The sum on the right-hand side is related to the static and high-frequency dielectric permittivities by [57]

$$\epsilon^0 = \epsilon^\infty + \frac{e^2}{4\pi\varepsilon_0}\frac{4\pi}{\Omega}\frac{\sum_\nu|\mathbf{Z}_\nu^*|^2}{M_0\omega_{\mathrm{TO}}^2}. \qquad (6)$$

Using this expression and the Lyddane-Sachs-Teller relation, $\epsilon^0/\epsilon^\infty = \omega_{\mathrm{LO}}^2/\omega_{\mathrm{TO}}^2$, Eq. (5) can be rewritten in the standard form [31]

$$|g(q)| = \alpha_{\mathrm{FR}}^{1/2}\hbar\omega_{\mathrm{LO}}\frac{q_{\mathrm{FR}}}{q}, \qquad (7)$$

where the dimensionless Fröhlich coupling strength α_{FR} is defined as [10]

$$\alpha_{\mathrm{FR}} = \frac{e^2}{4\pi\varepsilon_0}\frac{1}{\hbar}\sqrt{\frac{m^*}{2\hbar\omega_{\mathrm{LO}}}}\left(\frac{1}{\epsilon_\infty} - \frac{1}{\epsilon_0}\right), \qquad (8)$$

m^* is the band effective mass, and q_{FR} is a characteristic wave vector given by $q_{\mathrm{FR}}^2 = 4\pi\Omega^{-1}(\hbar/2m^*\omega_{\mathrm{LO}})^{1/2}$. Equations (3)

and (7) show that, in three dimensions, the Fröhlich interaction diverges as $1/q$, as is well known.

B. Fröhlich coupling in 2D systems

In early studies of polar electron-phonon coupling interactions in 2D systems, the Fröhlich matrix element was derived either within the strict 2D limit [43], or by considering electrons confined within an infinite square-well potential along the direction perpendicular to the slab (z direction in the following) [42].

The square-well approximations are arrived at by considering that, in calculations of physical properties, the 3D electron-phonon matrix element is modulated by the electron density along the z direction [21,42,48,58,59]:

$$|g^{2D}(\mathbf{q}_\|)|^2 = \frac{c}{2\pi}\int_{-\infty}^\infty dq_z \, F(q_z)|g^{3D}(\mathbf{q}_\|, q_z)|^2, \qquad (9)$$

where $\mathbf{q}_\|$ and q_z are the components of the phonon momentum $\mathbf{q}$ parallel and perpendicular to the slab, respectively, c is the slab thickness, and $F(q_z)$ is the Fourier component of the electron density profile along z, $F(z)$:

$$F(q_z) = \int_{-\infty}^\infty dz \, F(z)e^{-iq_z z}. \qquad (10)$$

When the electron is strictly confined in a 2D sheet of zero thickness, the profile becomes a Dirac delta function, $F(z) = \delta(z)$, and one obtains the 2D Fröhlich matrix elements in the strict 2D limit [27,42,48]. After integrating out the third dimension in Eq. (9), the matrix element is written as [42,48]

$$|g^{2D}(q_\|)| = \alpha_{\mathrm{FR}}^{1/2}\hbar\omega_{\mathrm{LO}}\frac{q_{\mathrm{FR}}(c/2)^{1/2}}{q_\|^{1/2}}, \qquad (11)$$

A similar result can alternatively be derived starting from the Coulomb potential in two dimensions [43]. At variance with the standard 3D Fröhlich matrix element, which scales as q^{-1}, the matrix elements in the strict 2D approximation scales as $q_\|^{-1/2}$. This singular behavior is currently understood to be an artifact of the model, which is inconsistent with experiments [60]. To overcome this limitation, Ref. [27] employed a Gaussian profile of width σ to described the electron density along the z direction. The resulting matrix element in the long-wavelength limits reads

$$|g^{2D}(\mathbf{q}_\|)| = g \, \mathrm{erfc}(q_\|\sigma/2), \qquad (12)$$

where the constants g and σ are determined by fitting this expression to *ab initio* data. This model has successfully been employed to investigate the transport properties of transition-metal dichalcogenide monolayers [27]. One potential limitation of this approach is that the relation between the electron-phonon coupling strength g and materials parameters such as dielectric constants, Born charges, and vibrational frequencies is not apparent as in the standard *ab initio* Fröhlich matrix element [32,33]. Being able to trace the coupling back to these properties would be desirable, so as to establish predictive analytical models for electron-phonon physics in two dimensions.

To bridge the gap between model studies of electron-phonon interactions in 2D materials and first-principle calculations, Ref. [26] developed a refined model which takes into

account microscopic features such as Born charges, phonon frequencies, and the dielectric permittivity of the 2D slab. In this model one assumes that the atomic displacements generate a uniform macroscopic polarization density within the slab. For brevity we quote the expression obtained by Ref. [26] for a 2D slab surrounded by vacuum (the general expression can be found in Ref. [26]):

$$|g^{2D}(q_\parallel)| = \frac{2\pi}{A} \frac{e^2}{4\pi\varepsilon_0} \left(\sum_\kappa \frac{\hbar}{2M_\kappa \omega_{LO}} Z_{\kappa,\parallel}^{*,2} \right)^{1/2} \frac{1}{\epsilon_\infty} \frac{2}{q_\parallel d}$$
$$\times \left[1 + \frac{\epsilon_\infty^{-1}}{q_\parallel d} \frac{e^{q_\parallel d} - 1}{1 - (1 + \epsilon_\infty^{-1})(1 + e^{q_\parallel d})/2} \right]. \quad (13)$$

In this expression, d and A are the slab thickness and unit-cell area, respectively, ϵ_∞ is the (isotropic) high-frequency permittivity, ω_{LO} is the frequency of the longitudinal-optical (LO) mode, and M_κ and $Z_{\kappa,\parallel}^*$ are the atomic masses and in-plane Born charges, respectively. As for Eq. (12), the coupling given by Eq. (13) is not singular for $q_\parallel \to 0$.

The model leading to Eq. (13) has successfully been employed in calculations of electron-phonon couplings in two dimensions [26,28,61] and constitutes the *de facto* state-of-the-art approach in the field. There have been at least two generalizations of the model of Ref. [26], which additionally take into account the out-of-plane polarization and the effect of exact 2D long-range screening [29,62]. However, all these approaches are designed to describe a 2D slab between two semi-infinite media. In some cases it may be desirable to model the 2D system as a periodic superlattice rather than an isolated slab, for example when studying van der Waals heterostructures or 2D semiconductor/insulator interfaces. In the next section we derive such a model for quasi-2D systems, by generalizing the approach developed in Ref. [32] for bulk crystals.

III. DERIVATION OF THE FRÖHLICH MATRIX ELEMENT IN QUASI-2D SYSTEMS

In this section we generalize the reasoning leading to Eq. (3) to the case of a periodic stack where two materials alternate along the z direction, as shown in Fig. 1. We label these materials as "primary" and "secondary" layer, respectively. We consider the primary layer to be the 2D slab of interest, and the secondary layer to be the embedding medium or subrate. For example the primary layer could be a monolayer of MoS_2, and the secondary layer could be multilayer BN or vacuum. We describe the secondary layer as a homogeneous dielectric medium, *without taking into account the discrete, atomic-scale structure of this layer*.

We denote the nominal thickness of the primary and secondary layer as d and D, respectively, and the unit cell length in the z direction as $c = d + D$. For convenience we shall say that the primary layer extends from $z = -d$ to $z = 0$, and the secondary layer occupies the region from $z = 0$ to $z = D$. The unit cell is repeated periodically within a Born–von Kármán (BvK) supercell consisting of multiple unit cells in the xy plane and in the z direction, and periodic boundary conditions on the BvK cell are applied.
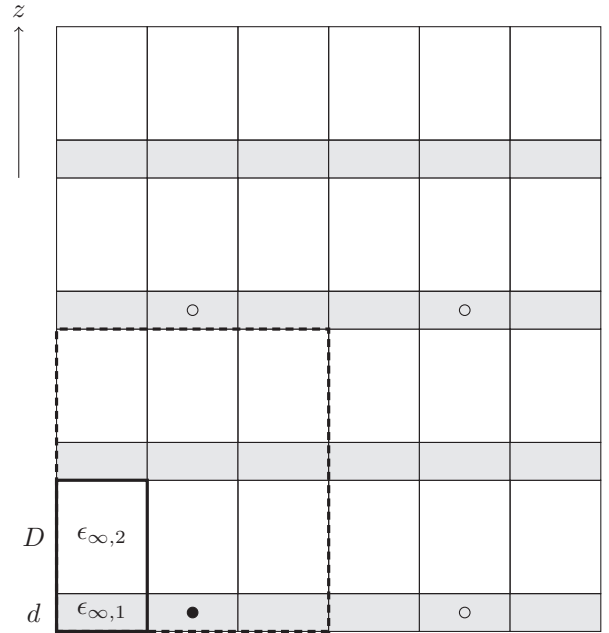

FIG. 1. Schematic representation of a superlattice consisting of a periodic stack of two layers alternating along the z direction. The material under consideration is the layer of thickness d and dielectric constant $\epsilon_{\infty,1}$. The the other layer, of thickness D and permittivity $\epsilon_{\infty,2}$, is a dielectric continuum. The thick solid line denotes the boundary of the primitive unit cell; the thick dashed line indicates the boundary of the BvK supercell. Equation (18) gives the electrostatic potential generated by a point charge located in one of the layers (indicated by the disk ●). To obtain a solution that is periodic in the BvK supercell, we superimpose the potential of all periodic images (indicated by the circle ○). From the displacements of these charges we obtain the dipole potential. Our Fröhlich matrix element in Eq. (34) is then obtained by summing over the dipoles associated with every atomic displacement.

To keep the theory as simple as possible, we assume that the two layers can be described by effective isotropic high-frequency (relative) dielectric permittivities $\epsilon_{\infty,1}$ and $\epsilon_{\infty,2}$, following the same line or reasoning as in Refs. [26]. In particular, we assume that the dielectric permittivity is given by

$$\epsilon_\infty(z) = \begin{cases} \epsilon_{\infty,1} & -d < z < 0 \\ \epsilon_{\infty,2} & 0 < z < D \end{cases}. \quad (14)$$

This assumption is legitimate because (1) we are interested only in the long-wavelength limit of the electron-phonon matrix element and (2) the out-of-plane dielectric permittivity can effectively be made equal to the in-plane permittivity via an appropriate choice of the thickness d [26]. Evidently there is no sharp boundary between the primary and secondary layer in real materials, and the dielectric permittivity evolves smoothly [63]. However, the notion of a sharp dielectric interface considerably simplifies the equations without affecting the final results.

To extend the reasoning of Ref. [32] to the present case, we evaluate the electrostatic potential of a point dipole located at the position τ in the primary layer. To this aim, we begin by determining the electrostatic potential of a point

charge e located at $\boldsymbol{\tau}$, *without* considering its periodic replicas. Subsequently, we proceed to *replicate* this charge in all BvK supercells in order to describe realistic first-principles calculations. Following the notation of Ref. [32] [see Eq. (S1) of that work], the electrostatic potential of a single charge *without* its replicas is obtained as the solution of the inhomogeneous Poisson's equation:

$$\epsilon_\infty(z)\nabla^2\varphi(\mathbf{r};\tau_z) + \frac{d\epsilon_\infty(z)}{dz}\frac{\partial\varphi(\mathbf{r};\tau_z)}{\partial z} = -\frac{e}{\varepsilon_0}\delta(\mathbf{r}-\tau_z\mathbf{u}_z),$$
(15)

where we have set $\tau_x = \tau_y = 0$ to start with. $\mathbf{u}_z$ is the unit vector along z, and $-d < \tau_z < 0$. To proceed we perform a Fourier integral for the in-plane coordinates:

$$\varphi(\mathbf{r};\tau_z) = \int d\mathbf{Q}_\parallel\, \varphi(z,\mathbf{Q}_\parallel;\tau_z)e^{i\mathbf{Q}_\parallel\cdot\mathbf{r}_\parallel},$$
(16)

where the $\mathbf{Q}_\parallel$'s denote in-plane wave vectors and $\mathbf{r}_\parallel$ is the position in the xy plane. After replacing Eq. (16) inside Eq. (15) we obtain the following equation for $\varphi(z,\mathbf{Q}_\parallel;\tau_z)$:

$$\epsilon_\infty(z)\frac{\partial^2\varphi}{\partial z^2} + \frac{d\epsilon_\infty(z)}{dz}\frac{\partial\varphi}{\partial z} - \mathbf{Q}_\parallel^2\epsilon_\infty(z)\varphi$$
$$= -\frac{e}{(2\pi)^2\varepsilon_0}\delta(z-\tau_z).$$
(17)

The exact solution of this equation with the two-step dielectric profile defined in Eq. (14) has been derived by Ref. [64], in the context of a study of excitons in periodic superlattices. The solution is

$$\varphi(z;\mathbf{Q}_\parallel;\tau_z)$$
$$= \frac{e}{2(2\pi)^2\varepsilon_0\epsilon_{\infty,2}Q_\parallel(\gamma^- - \gamma^+)}$$
$$\times \begin{cases} z > \tau_z: \\ [(\alpha+\gamma^+\beta)e^{Q_\parallel\tau_z} + (\beta+\gamma^+\alpha)e^{-Q_\parallel\tau_z}]\varphi_-(z,\mathbf{Q}_\parallel), \\ z < \tau_z: \\ [(\alpha+\gamma^-\beta)e^{Q_\parallel\tau_z} + (\beta+\gamma^-\alpha)e^{-Q_\parallel\tau_z}]\varphi_+(z,\mathbf{Q}_\parallel), \end{cases}$$
(18)

where $Q_\parallel = |\mathbf{Q}_\parallel|$ and the function $\varphi_\pm$ is defined as

$$\varphi_\pm(z,\mathbf{Q}_\parallel)$$
$$= \begin{cases} nc-d < z < nc: \\ e^{\pm n\eta}[(\alpha+\gamma^\pm\beta)e^{Q_\parallel(z-nc)} + (\beta+\gamma^\pm\alpha)e^{-Q_\parallel(z-nc)}] \\ nc < z < nc+D: \\ e^{\pm n\eta}[e^{Q_\parallel(z-nc)} + \gamma^\pm e^{-Q_\parallel(z-nc)}], \end{cases}$$
(19)

with n being an integer. The quantities α, β, $\gamma^\pm$, and η appearing in these expressions are defined as follows:

$$\alpha = (1 + \epsilon_{\infty,2}/\epsilon_{\infty,1})/2,$$
(20)

$$\beta = (1 - \epsilon_{\infty,2}/\epsilon_{\infty,1})/2,$$
(21)

$$\gamma^\pm = -\frac{e^{Q_\parallel D} - e^{\pm\eta}(\alpha e^{-Q_\parallel d} + \beta e^{Q_\parallel d})}{e^{-Q_\parallel D} - e^{\pm\eta}(\beta e^{-Q_\parallel d} + \alpha e^{Q_\parallel d})},$$
(22)

$$\eta = \cosh^{-1}\{\cosh[Q_\parallel(D-d)] + 2\alpha^2/(2\alpha-1)$$
$$\times \sinh(Q_\parallel D)\sinh(Q_\parallel d)\}.$$
(23)

For later reference, it is useful to note that the potential $\varphi(z,\mathbf{Q}_\parallel;\tau_z)$ transforms as follows upon translations of the atomic coordinate by a unit cell vector along the z axis:

$$\varphi(z,\mathbf{Q}_\parallel;\tau_z+R_z) = \varphi(z-R_z,\mathbf{Q}_\parallel;\tau_z).$$
(24)

This property follows immediately from Eq. (17).

In order to determine the complete 3D Fourier transform of the potential, we write

$$\varphi(\mathbf{r};\tau_z) = \int d\mathbf{Q}\, \varphi(\mathbf{Q};\tau_z)e^{i\mathbf{Q}\cdot\mathbf{r}},$$
(25)

and we compare this expression with Eq. (16) to obtain

$$\varphi(\mathbf{Q};\tau_z) = \frac{1}{2\pi}\int dz\,\varphi(z,\mathbf{Q}_\parallel;\tau_z)e^{-iQ_z z}.$$
(26)

As a consequence of Eq. (24), the potential $\varphi(\mathbf{Q};\tau_z)$ transforms like a Bloch function under translation by a unit cell vectors along the z axis:

$$\varphi(\mathbf{Q};\tau_z+R_z) = e^{iQ_z R_z}\varphi(\mathbf{Q};\tau_z).$$
(27)

At this point we can replace Eqs. (18)–(23) inside Eq. (26) and and evaluate the integral. After some algebra we find

$$\varphi(\mathbf{Q};\tau_z) = \frac{e}{2(2\pi)^3\varepsilon_0\epsilon_{\infty,2}Q_\parallel}K(\mathbf{Q},\tau_z),$$
(28)

where the kernel function $K(\mathbf{Q},\tau_z)$ is a rather involved combination of complex exponentials which, besides $\mathbf{Q}$ and τ_z, depend on the geometric and dielectric parameters of the stack, d, D, $\epsilon_{\infty,1}$, and $\epsilon_{\infty,2}$. The complete expression for the kernel is provided in Appendix; see Eq. (A1).

The electrostatic potential $\varphi(\mathbf{r};\tau_z)$ given by Eqs. (25) and (28) corresponds to a single charge in the dielectric stack. In order to impose BvK boundary conditions, we place this charge at $\boldsymbol{\tau}$ and replicate it in every BvK supercell. We call the resulting potential $\phi(\mathbf{r};\boldsymbol{\tau})$:

$$\phi(\mathbf{r};\boldsymbol{\tau}) = \sum_\mathbf{T}\varphi(\mathbf{r}-\mathbf{T};\boldsymbol{\tau}),$$
(29)

where the $\mathbf{T}$'s are the the lattice vectors of the BvK supercell. We note that, to avoid an unphysical divergence of the potential, we should add to Eq. (29) the potential of a neutralizing background. However, this contribution cancels out when evaluating the potential of point dipoles, therefore it can safely be ignored. Since the potential $\phi(\mathbf{r};\boldsymbol{\tau})$ is periodic in the supercell, we can expand it in a discrete Fourier series:

$$\phi(\mathbf{r};\boldsymbol{\tau}) = \sum_{\mathbf{q},\mathbf{G}\neq-\mathbf{q}}\phi_\mathbf{q}(\mathbf{G};\boldsymbol{\tau})e^{i(\mathbf{q}+\mathbf{G})\cdot\mathbf{r}},$$
(30)

where the $\mathbf{G}$'s denote the reciprocal lattice vectors of the unit cell, and the $\mathbf{q}$'s are the Bloch wave vectors commensurate with the BvK supercell. The $\mathbf{q}+\mathbf{G}=0$ term is not included as it is canceled by the neutralizing background. By combining Eqs. (25) and (28)–(30) we find

$$\phi_\mathbf{q}(\mathbf{G};\boldsymbol{\tau}) = \frac{e}{2\varepsilon_0\epsilon_{\infty,2}N\Omega}\frac{e^{-i(\mathbf{q}_\parallel+\mathbf{G}_\parallel)\cdot\boldsymbol{\tau}_\parallel}}{|\mathbf{q}_\parallel+\mathbf{G}_\parallel|}K(\mathbf{q}+\mathbf{G},\tau_z),$$
(31)

where Ω is the volume of the unit cell, and N is the number of unit cells in the BvK supercell.

The next step in our procedure is to evaluate the potential of a point dipole. This is achieved simply by taking the linear variation of $\phi(\mathbf{r}; \boldsymbol{\tau})$ with respect to $\boldsymbol{\tau}$:

$$\frac{\partial \phi(\mathbf{r}; \boldsymbol{\tau})}{\partial \boldsymbol{\tau}} \cdot \Delta \boldsymbol{\tau} = \sum_{\mathbf{q}, \mathbf{G} \neq -\mathbf{q}} e^{i(\mathbf{q}+\mathbf{G})\cdot\mathbf{r}} \frac{\partial \phi_{\mathbf{q}}(\mathbf{G}; \boldsymbol{\tau})}{\partial \boldsymbol{\tau}} \cdot \Delta \boldsymbol{\tau}, \quad (32)$$

where $|\Delta \boldsymbol{\tau}|$ is the dipole length. As in Ref. [32], we now consider one such dipole potential for each atom in the BvK supercell: the charge will be given by the Born effective charge tensor, and the direction and length of the dipole will be given by the atomic displacement pattern $\Delta \boldsymbol{\tau}^{(\mathbf{q}\nu)}$ in a phonon mode with wave vector $\mathbf{q}$:

$$\Delta V_{\mathbf{q}\nu}(\mathbf{G}) = -e \sum_{\kappa \mathbf{R}, \alpha\beta} \frac{\partial \phi_{\mathbf{q}}(\mathbf{G}; \boldsymbol{\tau}_{\kappa \mathbf{R}})}{\partial \tau_{\kappa \mathbf{R}\alpha}} Z^*_{\kappa, \alpha\beta} \Delta \tau^{(\mathbf{q}\nu)}_{\kappa \mathbf{R}\beta}. \quad (33)$$

The prefactor $-e$ has been added to obtain the potential energy experienced by an electron, and the atomic displacement in this expression is the same as in Eq. (2).

The electron-phonon matrix element $g_{mn\nu}(\mathbf{k}, \mathbf{q}) = \langle \psi_{m\mathbf{k}+\mathbf{q}} | \Delta_{\mathbf{q}\nu} V | \psi_{n\mathbf{k}} \rangle$ associated with the potential $\Delta V_{\mathbf{q}\nu}$ is finally obtained by combining Eqs. (33), (31), (2), and (27):

$$g_{mn\nu}(\mathbf{k}, \mathbf{q}) = \frac{e^2}{2\varepsilon_0 \epsilon_{\infty,2} \Omega} (\hbar/2\omega_{\mathbf{q}\nu})^{1/2} \sum_{\mathbf{G} \neq -\mathbf{q}} \frac{\langle u_{m\mathbf{k}+\mathbf{q}+\mathbf{G}} | u_{n\mathbf{k}} \rangle}{|\mathbf{q}_{\parallel} + \mathbf{G}_{\parallel}|}$$

$$\times \sum_{\kappa} M_{\kappa}^{-1/2} e^{-i(\mathbf{q}_{\parallel}+\mathbf{G}_{\parallel})\cdot\boldsymbol{\tau}_{\kappa\parallel}} \sum_{\alpha\beta} Z^*_{\kappa, \alpha\beta} e_{\kappa\beta, \nu}(\mathbf{q})$$

$$\times \left[\delta_{\alpha, \parallel} i(\mathbf{q}+\mathbf{G})_{\alpha} K(\mathbf{q}+\mathbf{G}, \tau_{\kappa z}) \right.$$

$$\left. - \delta_{\alpha, z} \frac{\partial K(\mathbf{q}+\mathbf{G}, \tau_{\kappa z})}{\partial \tau_{\kappa z}} \right]. \quad (34)$$

In this expression, we have taken into account the normalization $\psi_{n\mathbf{k}} = N^{-1/2} e^{i\mathbf{k}\cdot\mathbf{r}} u_{n\mathbf{k}}$, where $u_{n\mathbf{k}}$ is the Bloch-periodic part of the wave function, we used the perioidic gauge $\psi_{n\mathbf{k}} = \psi_{n\mathbf{k}+\mathbf{G}}$, and the braket $\langle \cdots \rangle$ integral is now performed over the unit cell of the stack. Equation (34) is the central result of this work. It constitutes the generalization of the *ab initio* Fröhlich electron-phonon matrix element, derived in Ref. [32] for bulk 3D crystals, to periodic superlattices where two slabs alternate. Equation (34) can be used (1) to improve the Wannier-Fourier interpolation of the electron-phonon matrix elements in the case of 2D materials, as shown in Refs. [32,33] for the 3D case and (2) to derive realistic analytical models of Fröhlich interactions in 2D and quasi-2D systems. In the remainder of this work we discuss both applications.

IV. THE LIMITS OF 3D BULK CRYSTAL, 2D SLAB IN VACUUM, AND ATOMICALLY THIN MONOLAYER IN VACUUM

In this section we show how Eq. (34) correctly reduces to the result of Ref. [32] in the limit of a single layer ($D = 0$), and to the result of Ref. [26] in the limit of a slab in vacuum ($D = \infty$ and $\epsilon_{\infty,2} = 1$). This latter situation would correspond, for example, to a suspended MoS$_2$ monolayer. To demonstrate the flexibility of our approach, we also consider a third option, namely an atomically thin monolayer in vacuum, where all the atoms have the same z coordinate; this is the case, for example, of monolayer h-BN.

A. The limit of a 3D bulk crystal

The Fröhlich matrix element for a 3D extended crystal is obtained by setting the thickness of the secondary layer to zero, $D = 0$, in Eq. (34). Since this parameter enters Eq. (34) only via the kernel $K(\mathbf{Q}, \tau_z)$, we start by considering this kernel.

In the limit of small D ($D \ll c$), we have $d = c$, $\eta = Q_{\parallel} c$ from Eq. (23), and $\gamma^+ = (\alpha - 1)/\alpha$, $\gamma^- = \alpha/(\alpha - 1)$. Using these relations inside in Eq. (A1), after some algebraic manipulations we obtain

$$\lim_{D \to 0} K(\mathbf{Q}, \tau_z) = 2 \frac{\epsilon_{\infty,2}}{\epsilon_{\infty,1}} \frac{Q_{\parallel}}{Q^2} e^{-iQ_z \tau_z}. \quad (35)$$

This expression can be replaced for the square brackets in Eq. (34). After this substitution, the matrix element for $D = 0$ reduces to

$$g_{mn\nu}(\mathbf{k}, \mathbf{q}) = i \frac{4\pi}{\Omega} \frac{e^2}{4\pi\varepsilon_0} \sum_{\kappa} (\hbar/2M_{\kappa}\omega_{\mathbf{q}\nu})^{1/2}$$

$$\times \sum_{\mathbf{G} \neq -\mathbf{q}} e^{-i(\mathbf{q}+\mathbf{G})\cdot\boldsymbol{\tau}_{\kappa}} \langle u_{m\mathbf{k}+\mathbf{q}+\mathbf{G}} | u_{n\mathbf{k}} \rangle$$

$$\times \sum_{\alpha\beta} \frac{(\mathbf{q}+\mathbf{G})_{\alpha} Z^*_{\kappa, \alpha\beta} e_{\kappa\beta, \nu}(\mathbf{q})}{\epsilon_{\infty,1} |\mathbf{q} + \mathbf{G}|^2}. \quad (36)$$

This result is essentially identical to the matrix element derived in Ref. [32] for bulk 3D crystals; see Eq. (3). The only difference is that, to keep the derivation tractable, in the present study we have replaced the anisotropic dielectric permittivity tensor by a scalar isotropic permittivity. A similar choice was made in Ref. [26].

In summary, the Fröhlich matrix element given by Eq. (34) correctly reduces to the bulk limit in the case of a 3D homogeneous dielectric.

B. The limit of an isolated 2D slab

The other important limit to be investigated corresponds to the case of the Fröhlich interaction for an isolated 2D slab embedded in a dielectric continuum. This limit is obtained by taking $D \gg d$ in Eq. (34). The case of an isolated slab in vacuum is further obtained by setting $\epsilon_{\infty,2} = 1$.

Taking the limit $D \gg d$ of the kernel function $K(\mathbf{Q}, \tau_z)$ given in Eq. (A1) requires a certain number of algebraic manipulations. Here we limit ourselves to remark that, in this limit, γ^+ remains finite, e^{η} scales as $e^{Q_{\parallel}D}$, and γ^- scales as $e^{2Q_{\parallel}D}$. We find

$$\lim_{D \gg d} K(\mathbf{Q}, \tau_z) = 2(\alpha - \beta) \frac{Q_{\parallel}}{Q_{\parallel}^2 + Q_z^2} \left\{ e^{-iQ_z \tau_z} + + \frac{\beta}{\alpha^2 e^{2Q_{\parallel}d} - \beta^2} \right.$$

$$\left. \times [e^{Q_{\parallel}\tau_z} f_1(\mathbf{Q}d) + e^{-Q_{\parallel}\tau_z} f_2(\mathbf{Q}d)] \right\}, \quad (37)$$

having defined

$$f_1(\mathbf{Q}d) = \alpha e^{2Q_\parallel d} + \beta e^{(Q_\parallel + iQ_z)d}, \tag{38}$$

$$f_2(\mathbf{Q}d) = \beta + \alpha e^{(Q_\parallel + iQ_z)d}. \tag{39}$$

In this form, the effect of reduced dimensionality is not apparent, and the kernel is singular at long wavelength as for the bulk 3D case. In order to see the effect of dimensionality we need to carry out the summation over G_z appearing in (34). Since the overlap integral $\langle u_{m\mathbf{k}+\mathbf{q}+\mathbf{G}}|u_{n\mathbf{k}}\rangle$ depends on G_z, we need to evaluate the sum

$$\sum_{G_z} \langle u_{m\mathbf{k}+\mathbf{q}+\mathbf{G}}|u_{n\mathbf{k}}\rangle K(\mathbf{Q}_\parallel, q_z + G_z, \tau_z). \tag{40}$$

If the wave functions are localized within a characteristic length comparable to the thickness d of the dielectric slab, and if we take the limit $D \gg d$, the overlap term $\langle u_{m\mathbf{k}+\mathbf{q}+\mathbf{G}}|u_{n\mathbf{k}}\rangle$ becomes only weakly dependent on G_z, and the summation can be carried out explicitly. The specific details of the wave function localization around the slab are not critical to the final result, but in order to make contact with Ref. [26] we follow their choice and we set the Bloch-periodic components of the wave functions to be normalized rectangular functions in the direction perpendicular to the slab:

$$u_{n\mathbf{k}}(\mathbf{r}) = \begin{cases} \sqrt{c/\Omega d} & -d < z < 0, \\ 0 & 0 < z < D. \end{cases} \tag{41}$$

The corresponding wave functions are products of plane waves and this rectangular function. This choice is legitimate since we are interested in the long-wavelength limit of the Fröhlich matrix element, therefore the details of the wave function at the atomic scale do not matter. With the above choice the overlap integral becomes

$$\langle u_{m\mathbf{k}+\mathbf{q}+\mathbf{G}}|u_{n\mathbf{k}}\rangle = \delta_{mn}\delta_{\mathbf{G}_\parallel,0}\frac{1 - e^{-iG_z d}}{iG_z d}. \tag{42}$$

The summation in Eq. (40) can now be carried out explicitly by combining Eqs. (37) and (42). Since we are interested in the limit $D \gg d$, we have that $q_z \to 0$, G_z becomes a continuous variable, and the summation over G_z can be replaced by an integral. After some algebra we find

$$\lim_{D \gg d} \sum_{G_z} \langle u_{m\mathbf{k}+\mathbf{q}+\mathbf{G}}|u_{n\mathbf{k}}\rangle K(\mathbf{Q}_\parallel, q_z + G_z, \tau_z)$$

$$= \delta_{mn}\delta_{\mathbf{G}_\parallel,0}\frac{c(\alpha - \beta)}{Q_\parallel d}\left[2 - e^{Q_\parallel \tau_z} - e^{-Q_\parallel \tau_z - Q_\parallel d}\right.$$

$$\left. + \frac{\beta(1 - e^{-Q_\parallel d})}{\alpha e^{Q_\parallel d} - \beta}(e^{Q_\parallel \tau_z}e^{Q_\parallel d} + e^{-Q_\parallel \tau_z})\right]. \tag{43}$$

The matrix element given in Ref. [26] was obtained by considering that the ionic polarization is distributed uniformly across the slab. Their choice can be incorporated in the present formalism by averaging the atomic positions τ_z over the slab thickness. To this aim, we define the kernel average as follows:

$$\langle K(\mathbf{Q}_\parallel, q_z + G_z) \rangle = \frac{1}{d}\int_{-d}^{0} d\tau_z K(\mathbf{Q}_\parallel, q_z + G_z, \tau_z). \tag{44}$$

By combining the last two equations and carrying out the integrals of the terms $e^{\pm Q_\parallel \tau_z}$, we obtain

$$\lim_{D \gg d} \sum_{G_z} \langle u_{m\mathbf{k}+\mathbf{q}+\mathbf{G}}|u_{n\mathbf{k}}\rangle \langle K(\mathbf{Q}_\parallel, q_z + G_z) \rangle$$

$$= \delta_{mn}\delta_{\mathbf{G}_\parallel,0}c\frac{2(2\alpha - 1)}{Q_\parallel d}\left[1 + \frac{1}{Q_\parallel d}\frac{(2\alpha - 1)(e^{Q_\parallel d} - 1)}{1 - \alpha(1 + e^{Q_\parallel d})}\right]. \tag{45}$$

Now we can replace this expression inside Eq. (34). We set $\epsilon_{\infty,1} = \epsilon_\infty$, $\epsilon_{\infty,2} = 1$, to find an expression for the Fröhlich 2D matrix element that is almost identical to the result of Ref. [26] as reported in Eq. (13) of the present work:

$$g_{mn\nu}(\mathbf{q}_\parallel) = i\delta_{mn}\frac{2\pi}{A}\frac{e^2}{4\pi\varepsilon_0}$$

$$\times \sum_{\kappa,\alpha=\parallel,\beta}\frac{q_\alpha}{q_\parallel}Z^*_{\kappa,\alpha\beta}\sqrt{\frac{\hbar}{2M_k\omega_{\mathbf{q}\nu}}}e^{-i\mathbf{q}_\parallel\cdot\boldsymbol{\tau}_\kappa\parallel}e_{\kappa\beta,\nu}(\mathbf{q}_\parallel)$$

$$\times \frac{1}{\epsilon_\infty}\frac{2}{q_\parallel d}\left[1 + \frac{\epsilon_\infty^{-1}}{q_\parallel d}\frac{e^{q_\parallel d} - 1}{1 - (1 + \epsilon_\infty^{-1})(1 + e^{q_\parallel d})/2}\right]. \tag{46}$$

Note that this expression contains only $\mathbf{q}_\parallel$ because we are in the limit $q_z \to 0$, and it no longer depends on the electron wave vector $\mathbf{k}$.

The equivalence between Eq. (46) and Eq. (13) can be made more apparent by introducing the mass-weighted mode-effective charge $Z^*_{\mathbf{q}_\parallel\nu}$ as follows:

$$Z^*_{\mathbf{q}_\parallel\nu} = \sum_\kappa \sqrt{\frac{M_0}{M_k}}\widehat{\mathbf{q}}_\parallel \cdot \mathbf{Z}^*_\kappa \cdot \mathbf{e}_{\kappa,\nu}(\mathbf{q}_\parallel)e^{-i\mathbf{q}_\parallel\cdot\boldsymbol{\tau}_\kappa\parallel}, \tag{47}$$

where $\widehat{\mathbf{q}}_\parallel$ is the unit vector in the direction of $\mathbf{q}_\parallel$. Using this definition, Eq. (46) can be rewritten more compactly as

$$g_{mn\nu}(\mathbf{q}_\parallel) = i\delta_{mn}\frac{2\pi}{A}\frac{e^2}{4\pi\varepsilon_0}\sqrt{\frac{\hbar}{2M_0\omega_{\mathbf{q}\nu}}}Z^*_{\mathbf{q}_\parallel\nu}\frac{1}{\epsilon_\infty}\frac{2}{q_\parallel d}$$

$$\times \left[1 + \frac{\epsilon_\infty^{-1}}{q_\parallel d}\frac{e^{q_\parallel d} - 1}{1 - (1 + \epsilon_\infty^{-1})(1 + e^{q_\parallel d})/2}\right]. \tag{48}$$

Equation (13) is recovered by taking the $\mathbf{q}_\parallel \to 0$ limit of $Z^*_{\mathbf{q}_\parallel\nu}/\omega_{\mathbf{q}\nu}^{1/2}$, and by adding the square moduli of the matrix elements for the two in-plane directions of the zone-center longitudinal optical modes.

C. The limit of an isolated 2D monolayer where all atoms have the same z coordinate

An alternative expression to the 2D Frhölich matrix element can be obtained in the limit of materials consisting of a single atomic layer where all atoms have the same τ_z, such as for example monolayer boron nitride.

In this scenario we can go back to Eq. (43), and instead of averaging τ_z over the dielectric slab (which is equivalent to the approach of Ref. [26] as shown in Sec. IV B), we can simply set $\tau_z = -d/2$ for all atoms, which corresponds to having the

monolayer in the middle of the dielectric slab. We find

$$\lim_{D\gg d} \sum_{G_z} \langle u_{m\mathbf{k}+\mathbf{q}+\mathbf{G}}|u_{n\mathbf{k}}\rangle K(\mathbf{Q}_\|, q_z + G_z, \tau_z = -d/2)$$

$$= \delta_{mn}\delta_{\mathbf{G}_\|,0}\frac{2(2\alpha-1)c}{Q_\| d}\left[1 + \frac{(2\alpha-1)e^{Q_\| d/2}}{1-\alpha(e^{Q_\| d}+1)}\right]. \quad (49)$$

By repeating the same steps that led to Eq. (46) in the slab case, we obtain the Fröhlich matrix element for an isolated 2D monolayer:

$$g_{mn\nu}(\mathbf{q}_\|) = i\delta_{mn}\frac{2\pi}{A}\frac{e^2}{4\pi\varepsilon_0}\sqrt{\frac{\hbar}{2M_0\omega_{\mathbf{q}\nu}}}Z_{\mathbf{q}_\|\nu}^*\frac{1}{\epsilon_\infty}\frac{2}{q_\| d}$$

$$\times \left[1 + \frac{\epsilon_\infty^{-1}e^{q_\| d/2}}{1-(1+\epsilon_\infty^{-1})(1+e^{q_\| d})/2}\right]. \quad (50)$$

In the limit of long wavelengths, this expression reduces to the simplified form

$$\lim_{q_\|\to 0} g_{mn\nu}(\mathbf{q}_\|) = i\delta_{mn}\frac{2\pi}{A}\frac{e^2}{4\pi\varepsilon_0}\sqrt{\frac{\hbar}{2M_0\omega_{\mathbf{q}\nu}}}Z_{\mathbf{q}_\|\nu}^*\frac{1}{1+q_\|/q_0},$$
$$(51)$$

having defined

$$q_0 = \frac{4\epsilon_\infty}{2\epsilon_\infty^2 - 1}\frac{1}{d}. \quad (52)$$

This approximation to Eq. (50) remains very close to the the original equation through the entire range of wave vectors $q_\|$, therefore this simplified matrix element is especially useful to derive analytic expressions for the Frhöhlich coupling in two dimensions.

V. MODEL MATRIX ELEMENTS WITHOUT BORN EFFECTIVE CHARGES

The 2D Fröhlich matrix element for isolated slabs and monolayers as derived in Eqs. (48), (50), and (51) can be simplified further by expressing the mode effective Born charges in terms of the dielectric constants of the slab. This step is useful to obtain the 2D analog of the Fröhlich matrix element used for bulk 2D solids, Eq. (7).

In the long-wavelength limit, the relation between dielectric constants and the mode effective charges is provided by Eq. (56) of Ref. [57], here rewritten without assuming Hartree units (in the following we use $\epsilon_\infty, \epsilon_0$ or $\epsilon^\infty, \epsilon^0$ interchangeably to accommodate the other indices as needed):

$$\epsilon_{\hat{\mathbf{q}}_\|}^0 - \epsilon_{\hat{\mathbf{q}}_\|}^\infty = \frac{e^2}{4\pi\varepsilon_0}\frac{4\pi}{\Omega}\sum_\nu\frac{(Z_{\hat{\mathbf{q}}_\|,\nu}^*)^2}{M_0\omega_{0,\nu}^2}. \quad (53)$$

In this expression, $\epsilon_{\hat{\mathbf{q}}_\|}^0$ and $\epsilon_{\hat{\mathbf{q}}_\|}^\infty$ denote the relative static and high-frequency dielectric permittivities evaluated along the direction $\hat{\mathbf{q}}_\|$, and $\omega_{0,\nu}$ indicates the frequency of the ν vibrational mode at $\mathbf{q} = 0$. This frequency *does not* include the nonanalytic part of the dynamical matrix, i.e., it is the TO frequency.

To make contact with the standard Fröhlich model for 3D bulk systems, we must convert the TO frequencies in Eq. (53) into LO frequencies. This can be achieved via the generalized

Lyddane-Sachs-Teller relations, namely, Eq. (64) of Ref. [57]:

$$\prod_\nu\frac{\omega_{\mathbf{q}_\|\to 0,\nu}^2}{\omega_{\mathbf{q}_\|=0,\nu}^2} = \frac{\epsilon_{\hat{\mathbf{q}}_\|}^0}{\epsilon_{\hat{\mathbf{q}}_\|}^\infty}. \quad (54)$$

The frequencies in the denominator of this expression are the TO frequencies, and those in the numerator are the LO frequencies. By combining Eqs. (53) and (54), and considering a single infrared-active mode, we find

$$\frac{(Z_{\hat{\mathbf{q}}_\|,\nu}^*)^2}{\omega_{\mathbf{q}_\|\to 0,\nu}} = \frac{\varepsilon_0\Omega M_0}{e^2}\omega_{\mathbf{q}_\|\to 0,\nu}(\epsilon_{\hat{\mathbf{q}}_\|}^\infty)^2\left(\frac{1}{\epsilon_{\hat{\mathbf{q}}_\|}^\infty} - \frac{1}{\epsilon_{\hat{\mathbf{q}}_\|}^0}\right). \quad (55)$$

This relation should be replaced inside Eqs. (48), (50), and (51), after noting that the frequency $\omega_{\mathbf{q}\nu}$ appearing in those expressions corresponds to $\omega_{\mathbf{q}_\|\to 0,\nu}$, i.e., the LO frequency.

The dielectric constants in Eq. (55) correspond to the entire supercell. In order to disentangle the screening by the dielectric slab and by the environment, we use the standard rule for a stack of dielectrics:

$$d\,\epsilon_1 + D\,\epsilon_2 = (d+D)\,\epsilon_{\hat{\mathbf{q}}_\|}. \quad (56)$$

After replacing these expression in Eq. (55), taking the limit $D \gg d$, and setting $\epsilon_1 = \epsilon$ and $\epsilon_2 = 1$, we find

$$\frac{(Z_{\hat{\mathbf{q}}_\|,\nu}^*)^2}{\omega_{\mathbf{q}_\|\to 0,\nu}} = \frac{\varepsilon_0 A d M_0}{e^2}\omega_{\mathrm{LO}}(\epsilon_0 - \epsilon_\infty), \quad (57)$$

where the LO frequency is given by $\omega_{\mathbf{q}_\|\to 0,\nu} = \omega_{\mathrm{LO}}$. The left-hand side is now expressed in terms of intrinsic properties of the slab and does not depend on the size of the vacuum buffer. We also note that the Born charge evaluated along the direction parallel to the slab does not depend on the size c of the supercell [65].

Incidentally, we remark that in the limit of $D \gg d$ the LO and TO frequencies tend to the same value, because the dielectric constant of the vacuum buffer (or any uniform dielectric buffer) overwhelms the dielectric screening of the slab. This is easily proven by replacing Eq. (56) inside Eq. (54) and taking the limit $D \gg d$. This observation is in agreement with the absence of LO-TO splitting in 2D materials discussed in Ref. [66].

Using Eq (57), we can now rewrite Eqs. (48), (50), and (51) without resorting to the Born charges:

$$g_{mn\nu}(\mathbf{q}_\|) = i\delta_{mn}\left[\frac{\pi}{2}\frac{e^2}{4\pi\varepsilon_0}\frac{d}{A}\hbar\omega_{\mathrm{LO}}(\epsilon_0 - \epsilon_\infty)\right]^{1/2}f(q_\| d, \epsilon_\infty),$$
$$(58)$$

where the dimensionless function $f(q_\| d, \epsilon_\infty)$ depends on the chosen approximation for the slab. The function corresponding to the model of Ref. [26] that yields Eq. (48) is

$$f_1(q_\| d, \epsilon^\infty) = \frac{1}{\epsilon_\infty}\frac{2}{q_\| d}\left[1 + \frac{\epsilon_\infty^{-1}}{q_\| d}\right.$$

$$\left.\times\frac{e^{q_\| d} - 1}{1-(1+\epsilon_\infty^{-1})(1+e^{q_\| d})/2}\right]. \quad (59)$$

The function corresponding to the present monolayer model that yields Eq. (50) is

$$f_2(q_\parallel d, \epsilon_\infty) = \frac{1}{\epsilon_\infty} \frac{2}{q_\parallel d} \left[1 + \frac{\epsilon_\infty^{-1} e^{q_\parallel d/2}}{1 - (1 + \epsilon_\infty^{-1})(1 + e^{q_\parallel d})/2} \right],$$
(60)

and last the function corresponding to the long-wavelength limit of the monolayer model, yielding Eq. (51), is

$$f_3(q_\parallel d, \epsilon_\infty) = \frac{1}{1 + q_\parallel/q_0},$$
(61)

with q_0 given by Eq. (52).

These expressions can be used to study Fröhlich interactions in two dimensions without performing explicit *ab initio* calculations. For the reader's convenience, we quote in full the expression corresponding to the simplest approximation, Eq. (61):

$$g_{mn\nu}(\mathbf{q}_\parallel) = i\delta_{mn} \left[\frac{\pi}{2} \frac{e^2}{4\pi\varepsilon_0} \frac{d}{A} \hbar\omega_{LO}(\epsilon_0 - \epsilon_\infty) \right]^{1/2} \frac{q_0}{q_0 + q_\parallel},$$
(62)

where q_0 is given by Eq. (52), which we reproduce here for convenience:

$$q_0 = \frac{4\epsilon_\infty}{2\epsilon_\infty^2 - 1} \frac{1}{d}.$$
(63)

The key difference between this expression and the 3D Fröhlich matrix element in Eqs. (7) and (8) is that the limit $\mathbf{q}_\parallel \to 0$ is finite, as expected.

VI. METHODS AND RESULTS

A. Computational details

In order to demonstrate the method outlined in Secs. III–V, we consider hexagonal boron nitride (h-BN) and molybdenum disulfide (MoS$_2$) as test systems. Both compounds crystallize in a layered hexagonal structure with space group P6$_3$/mmc. We performed calculations of the ground state electronic structure and phonon dispersions using density-functional theory and density-functional perturbation theory, using plane waves and pseudopotentials, as implemented in the QUANTUM ESPRESSO materials simulation suite [67,68]. We used ONCV pseudopotentials [69,70] (h-BN: PBE [71]; MoS$_2$: LDA [72,73]), with plane waves kinetic energy cutoffs of 125 Ry and 135 Ry, respectively. In both cases, the Brillouin zone grid was sampled by using a Γ-centered uniform grid of $14 \times 14 \times 6$ points [74]. The lattice vectors and internal coordinates of the bulk crystals were optimized with this setup. DFPT calculations of phonons and electron-phonon couping matrix elements were performed using both a periodic supercell geometry, and using 2D Coulomb truncation [75]. The interpolation of the matrix elements [35] was performed using the WANNIER90 [76] and EPW [77] codes.

To build the monolayer models, we start from bulk crystals of h-BN and MoS$_2$, we remove one of the two layers in the crystalling unit cell, and we expand the vacuum gap in the z direction to $c = 20$ Å. With this choice, the direct gap nature of the monolayers is correctly captured. Soft phonons

TABLE I. Calculated material parameters of monolayer h-BN and monolayer MoS$_2$. m_e and e are the electron mass and charge, respectively. ω_{LO}^{2D} is the phonon energy calculated using 2D Coulomb truncation. The calculation of the dielectric thickness d and the effective dielectric constants ϵ^∞ and ϵ^0 is discussed in Sec. VI B.

	Property	Symbol	Value	Unit
h-BN	Lattice constant	a	2.511	Å
	Aspect ratio	c/a	7.965	
	Effective mass	$m_{h,\parallel}^*$	0.650	m_e
	Base area of unit cell	A	5.460	Å^2
	Born charge	$Z_\parallel^*(B)$	2.702	e
		$Z_\parallel^*(N)$	−2.702	e
	LO phonon energy	$\hbar\omega_{LO}$	181.560	meV
		$\hbar\omega_{LO}^{2D}$	166.992	meV
	Dielectric thickness	d	2.648	Å
	High-frequency permittivity	ϵ_∞	5.695	
	Low-frequency permittivity	ϵ_0	7.921	
MoS$_2$	Lattice constant	a	3.123	Å
	Aspect ratio	c/a	6.404	
	Effective mass	$m_{h,\parallel}^*$	0.570	m_e
	Base area of unit cell	A	8.446	Å^2
	Born charge	$Z_\parallel^*(Mo)$	−1.170	e
		$Z_\parallel^*(S)$	0.585	e
	LO phonon energy	$\hbar\omega_{LO}$	48.734	meV
		$\hbar\omega_{LO}^{2D}$	48.419	meV
	Dielectric thickness	d	5.468	Å
	High-frequency permittivity	ϵ_∞	16.424	
	Low-frequency permittivity	ϵ_0	16.672	

corresponding to the interlayer breathing mode are found for $8 \times 8 \times 1$ and $12 \times 12 \times 1$ Brillouin zone grids. To avoid these soft modes, we start from a coarser $4 \times 4 \times 1$ grid. This choice, albeit approximate, does not affect the long-range Fröhlich component of the electron-phonon matrix element. The in-plane lattice parameters were set to the values optimized the corresponding bulk crystals, namely, $a = 2.51$ Å for h-BN and $a = 3.12$ Å for MoS$_2$. In Table I we report the calculated structural parameters, band effective masses, Born charges, and phonon energies. These values agree with previous literature [78,79].

B. Validation of the formalism against explicit DFPT calculations

In this section we validate our formulation of the Fröhlich matrix element in a slab geometry, by comparing our expression (34) to explicit DFPT calculations. We consider two types of calculations: (1) DFPT calculations in a periodic supercell configuration and (2) DFPT calculations using Coulomb truncation, which are meant to describe an isolated monolayer without periodic images. We recall that Eq. (34) is a completely general expression that should be able to reproduce both of these scenarios.

The kernel appearing in Eq. (34) and reported in Eq. (A1) depends on the values $\epsilon_{\infty,1}$, $\epsilon_{\infty,2}$, and d that define the dielectric profile; see Eq. (14). To extract these quantities from DFPT calculations, we use a simple capacitor stack model following Refs. [80] and [81]. The dielectric constant of the
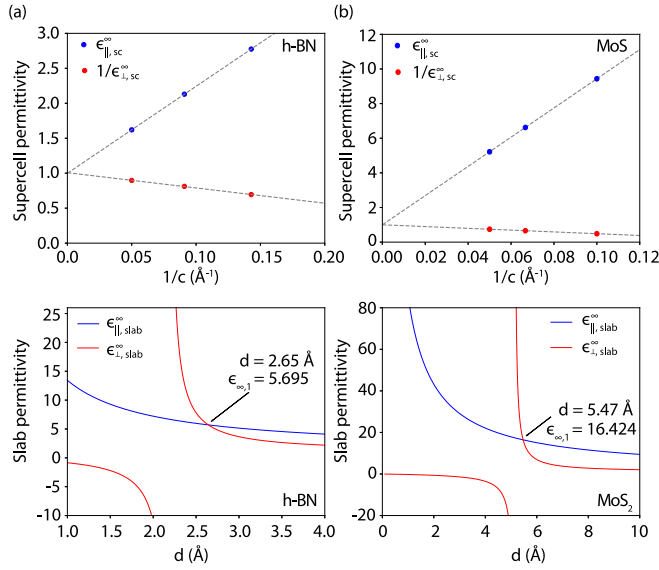
FIG. 2. (a, b) Calculated high-frequency dielectric constants of h-BN (a) and MoS_2 (b) monolayers in a supercell geometry, as a function of cell length $c = d + D$ along the z direction. See Fig. 1 for details of the supercell construction. The dashed straight lines are guides to the eye and show that the supercell permittivity scale linearly with $1/c$. (c, d) Dielectric constants of monolayer h-BN (c) and MoS_2 (d), as extracted from Eqs. (64) and (65), as a function of the dielectric thickness d. The crossing of the curves for the parallel and the perpendicular dielectric constants identify the effective dielectric thickness and permittivity of each slab. The symbols $\parallel$ and $\perp$ indicate dielectric constant parallel and perpendicular to the slab surface, respectively.

supercell can be written in terms of the dielectric constants of the slab and the dielectric environment as

$$c\,\epsilon_{\parallel}^{\mathrm{sc}} = D\epsilon_{\parallel}^{\mathrm{env}} + d\,\epsilon_{\parallel}^{\mathrm{slab}}, \qquad (64)$$

$$c\,\epsilon_{\perp,\mathrm{sc}}^{-1} = D\epsilon_{\perp,\mathrm{env}}^{-1} + d\,\epsilon_{\perp,\mathrm{slab}}^{-1}. \qquad (65)$$

In these expressions, "sc" refers to the supercell, "env" stands for the environment (e.g., vacuum), and "slab" stands for the 2D layer; $\parallel$ and $\perp$ refer to the dielectric constants in the direction parallel and perpendicular to the layer, respectively. The values $\epsilon_{\parallel}^{\mathrm{sc}}$ and $\epsilon_{\perp}^{\mathrm{sc}}$ are obtained from DFPT calculations on the supercell, while the values $\epsilon_{\parallel,\mathrm{slab}}^{-1}$, $\epsilon_{\perp,\mathrm{slab}}^{-1}$, and d need to be extracted from Eqs. (64) and (65). In the following we consider a vacuum buffer, so that $\epsilon_{\parallel}^{\mathrm{env}} = \epsilon_{\perp}^{\mathrm{env}} = 1$.

To verify Eqs. (64) and (65), in Figs. 2(a) and 2(b) we plot the dielectric constants of supercells containing an h-BN (a) and a MoS_2 (b) monolayer as a function of the c parameter. In agreement with the above equations, the dielectric constants of the supercell vary linearly with c. While Eqs. (64) and (65) do not uniquely define $\epsilon_{\parallel,\mathrm{slab}}^{-1}$ and $\epsilon_{\perp,\mathrm{slab}}^{-1}$, we can introduce one additional relation to be consistent with the assumption of isotropic permittivity used in Eq. (14):

$$\epsilon_{\perp,\mathrm{slab}} = \epsilon_{\parallel,\mathrm{slab}}. \qquad (66)$$

This relation is justified on the grounds that our matrix elements is designed to capture the long-range behavior of the Fröhlich interaction, as already discussed in Ref. [26]. Taken
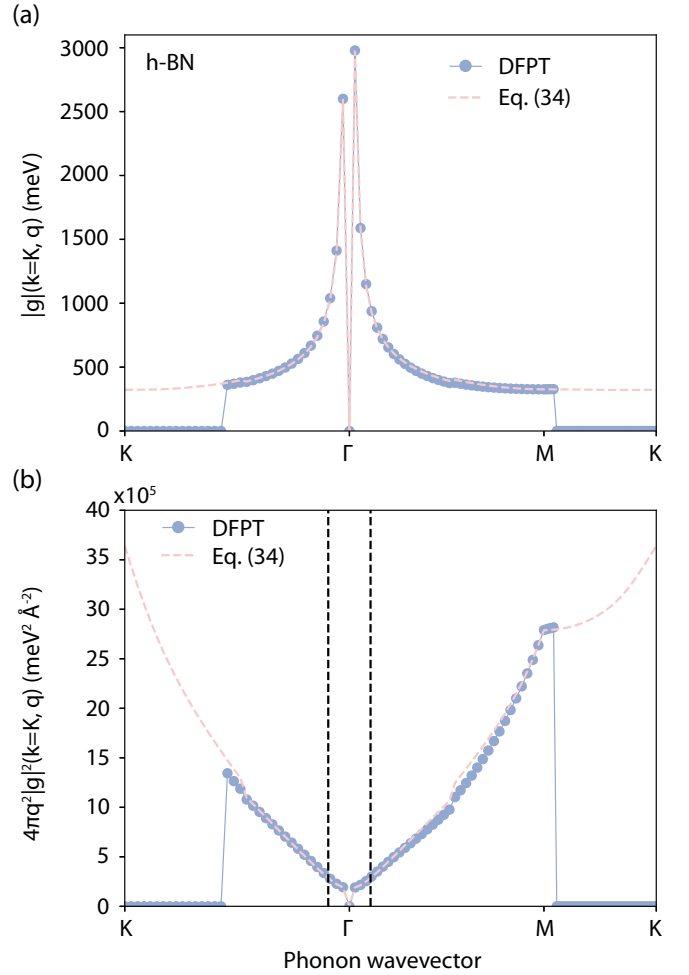

FIG. 3. (a) Electron-phonon matrix elements of monolayer h-BN calculated along a high-symmetry path in the 2D Brillouin zone. We report the results of explicit DPFT calculations (blue disks) and calculations using the matrix element in Eq. (34) (pink lines). In both cases we show the average of $|g_{mn\nu}(\mathbf{k}, \mathbf{q}_{\parallel})|^2$ over the TO and LO modes to avoid the discontinuity resulting from crossing phonon bands, $|g| = [\sum_{\nu} |g_{mn\nu}(\mathbf{k}, \mathbf{q})|^2]^{1/2}$, for m, n, $\mathbf{k}$ corresponding to the valence band maximum at the K point. The calculations were performed by using a supercell with a monolayer of h-BN and a vacuum buffer, with a total size $c = 20$ Å along the z direction. (b) Same raw data as in (a), but this time the matrix element is scaled by the phase-space volume element in three dimensions, $4\pi |\mathbf{q}_{\parallel}|^2 |g_{mn\nu}(\mathbf{k}, \mathbf{q}_{\parallel})|^2$. The vertical dashed lines indicate wave vectors such that $|\mathbf{q}_{\parallel}| = \pi/c$.

together, Eqs. (64)–(66) uniquely define the dielectric constants of the slab. A graphical solution of these equations is shown in Figs. 2(c) and 2(d) for h-BN and MoS_2, respectively. The effective dielectric thickness of the slabs and the associated dielectric constants are reported in Table I.

In Fig. 3 we compare the Fröhlich matrix element obtained for the h-BN monolayer in two ways: (1) Using the present formalism, as expressed by Eq. (34) (pink dash line) and (2) Using explicitly DFPT calculations in a periodic supercell *without* Coulomb truncation (light purple discs). The unit cell size along the z direction in these calculations is $d = 20$ Å. In Fig. 3(a) we show the modulus of the matrix element, $|g_{mn\nu}(\mathbf{k}, \mathbf{q}_{\parallel})|$, for m, n, $\mathbf{k}$ corresponding to the valence band

maximum at the K point, ν corresponding to the LO mode, and $\mathbf{q}_{\parallel}$ along a high-symmetry path. We see that our formalism matches the explicit DFPT calculations near $\mathbf{q} = 0$, thereby confirming the validity of our approach. Our Fröhlich matrix element also matches DPFT calculations away from the zone center, which indicates that the interaction of the highest optical mode in monolayer h-BN system is Fröhlich-like in a large portion of the Brillouin zone.

Figure 3(a) also shows that, although the supercell size in the z direction is as large as $c = 20$ Å, the matrix element preserves the signature of 3D Fröhlich coupling, as it can be seen from the near-singular behavior for $\mathbf{q}$ approaching the zone center. This effect is best visualized by considering the square modulus of the matrix element scaled by the phase-space volume element in three dimensions, $|g_{mn\nu}(\mathbf{k}, \mathbf{q})|^2 d\mathbf{q}$. This is the relevant quantity in applications, because typical expressions for electron self-energies, carrier mobilities, and superconducting gap function, as reported, e.g., in Ref. [1], all contain an integration of the type

$$\sum_{\nu} \int \frac{d\mathbf{q}}{\Omega_{\mathrm{BZ}}} |g_{mn\nu}(\mathbf{k}, \mathbf{q})|^2 f_{mn\nu}(\mathbf{k}, \mathbf{q}), \qquad (67)$$

where Ω_{BZ} is the volume of the Brillouin zone, and the function $f_{mn\nu}(\mathbf{k}, \mathbf{q})$ depends on the specific application. Figure 3(b) shows that $|g_{mn\nu}(\mathbf{k}, \mathbf{q})|^2 d\mathbf{q}$ scales as $|\mathbf{q}_{\parallel}|^1$ for $|\mathbf{q}_{\parallel}| > \pi/c$, and tends to a constant value for $|\mathbf{q}_{\parallel}| < \pi/c$. The implication is that, for $|\mathbf{q}_{\parallel}| > \pi/c$ the coupling is markedly different from the standard 3D Fröhlich interaction, while for $|\mathbf{q}_{\parallel}| < \pi/c$ the coupling is of Fröhlich type and diverges as $|\mathbf{q}_{\parallel}|^{-1}$. This singularity is a remnant of the Fröhlich interaction in three dimensions and originates from the periodic images of the atomic dipoles along the z direction. Indeed, to phonons with wavelengths longer than c, the supercell appears as a uniform material, for which the standard 3D Fröhlich interaction applies. In line with this residual 3D-type interaction, we find a small but nonvanishing LO-TO splitting in the phonon dispersion relations [$\hbar(\omega_{\mathrm{LO}} - \omega_{\mathrm{TO}}) = 15$ meV], whereas it is known that for a 2D system in isolation such a splitting is forbidden at the zone center [66].

The take-home message from Fig. 3 is that Eq. (34) correctly reproduces the Fröhlich matrix element in quasi-2D systems consisting of slab/vacuum stacks within periodic BvK boundary conditions. Therefore our expression makes it possible to perform calculations of electron-phonon interactions using Wannier interpolation [77] as for 3D materials, without requiring Coulomb truncation.

Now we move to the comparison between our formalism and DPFT calculations employing 2D Coulomb truncation. In Fig. 4 we compare the Fröhlich matrix element calculated for monolayer h-BN and MoS$_2$ via DFPT and Coulomb truncation [26] (blue disks) with our formalism (pink lines). In particular, we use the 2D kernel function Eq. (37), which corresponds to the $D \gg d$ limit of the exact matrix element in Eq. (34), as discussed in Sec. IV B. Figure 4(a) shows the modulus of the matrix element $|g_{mn\nu}(\mathbf{k}, \mathbf{q}_{\parallel})|$ for monolayer h-BN, with $m, n, \mathbf{k}$ set to the valence band maximum at the K point, ν corresponding to the LO mode, and $\mathbf{q}_{\parallel}$ along a high-symmetry path. Figure 4(b) shows the corresponding quantity for monolayer MoS$_2$, also for the top of the valence band at K.
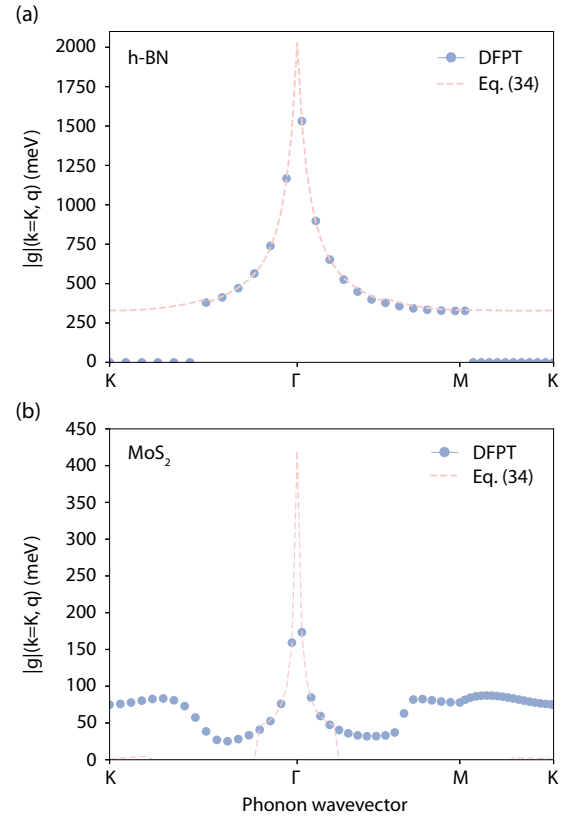

FIG. 4. (a) Electron-phonon matrix elements of monolayer h-BN calculated along a high-symmetry path in the 2D Brillouin zone, for infinite interlayer separation. We report the results of explicit DPFT calculations employing 2D Coulomb truncation (blue disks) and calculations using the matrix element in Eq. (34) with 2D kernel [Eq. (37)] (pink lines). In both cases we show the average of $|g_{mn\nu}(\mathbf{k}, \mathbf{q}_{\parallel})|^2$ over the TO and LO modes to avoid the discontinuity resulting from crossing phonon bands, $|g| = [\sum_{\nu}|g_{mn\nu}(\mathbf{k}, \mathbf{q})|^2]^{1/2}$. In this expression, $m, n, \mathbf{k}$ correspond to the valence band maximum at the K point. (b) Same as in (a), but for monolayer MoS$_2$ and infinite interlayer separation.

In both cases, we see that our formalism in the $D \gg d$ limit correctly reproduces the results of explicit 2D DFPT calculations. In particular, now that the size of the vacuum buffer tends to infinity, our formalism yields a finite, nonsingular Fröhlich matrix element at the zone center, in complete agreement with truncated DFPT calculations. The level of agreement that can be seen in Figs. 3 and 4 demonstrates the accuracy of our approach and shows that our method works seamlessly for periodic supercell calculations with finite vacuum buffer and for truncated 2D calculations with infinite vacuum.

It might be worth to point out that our matrix element is designed to describe the long-wavelength limit of $g_{mn\nu}(\mathbf{k}, \mathbf{q}_{\parallel})$, therefore a deviation between our results and DFPT calculations at large $\mathbf{q}_{\parallel}$ in Figs. 3 and 4 is expected. This deviation merely indicates that, at large $\mathbf{q}_{\parallel}$, the coupling mechanism is no longer of Fröhlich type. To describe the matrix element accurately throughout the Brillouin zone, it is sufficient to combine the present formalism with Wannier-Fourier interpolation, as already demonstrated in Ref. [32].
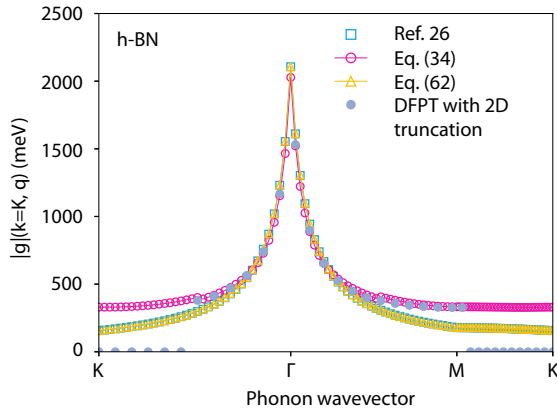
FIG. 5. Comparison between various models of the Fröhlich matrix elements for monolayer h-BN, in the limit of infinite vacuum size. We show the modulus of the matrix element, $|g_{mn\nu}(\mathbf{k}, \mathbf{q}_\parallel)|$, for $m, n, \mathbf{k}$ corresponding to the valence band maximum at the K point, and ν corresponding to the LO mode. The gray disks are the reference DFPT calculations using 2D Coulomb truncation. The data calculated using the method of Ref. [26] are shown as blue squares. The data obtained with our exact matrix element Eq. (34) are in magenta. The simplified model of Eq. (62), using the parameters in Table I, is shown as yellow triangles.

Next, we validate the simplified analytical model for 2D Fröhlich interactions given by Eq. (62). We recall that this model is useful to replace explicit DFPT calculations by a model matrix element that depends only on macroscopic properties such as dielectric constants, dielectric thickness, and phonon energy. Using the parameters in Table I for h-BN, we obtain the yellow triangles in Fig. 5. These values are compared to the corresponding matrix elements according to the method of Ref. [26] (blue squares), to our exact matrix element Eq. (34) (magenta disks), and to DFPT calculations using 2D Coulomb truncation (gray disks). It is apparent that, in the long-wavelength region, all these approaches are in very close agreement to each other. This successful comparison further demonstrates the validity of our approach and provides additional cross-validation of previously proposed approaches [26].

C. Evolution of the Fröhlich coupling from 3D to 2D

In this section, we discuss the transition of the polar Fröhlich coupling from 3D to 2D using the matrix element in Eq. (34). To keep the focus on the essential physics, we use the rectangular profile for the electron wave functions, as given by Eq. (41), and we employ materials parameter for h-BN, as reported in Table I.

Figure 6(a) shows the modulus of the electron-phonon matrix element, $|g_{mn\nu}(\mathbf{k}, \mathbf{q}_\parallel)|$, for m, n, ν corresponding to the valence band top of h-BN at the K point. We consider phonon wave vectors along the ΓM path (the curves along the ΓK path look very similar as already seen in Figs. 3–5). In Fig. 6 we compare the matrix elements obtained for various supercell sizes c along the z direction, including $c = 20$ Å (green), 40 Å (yellow), 140 Å (orange), and $c \rightarrow \infty$ (blue).
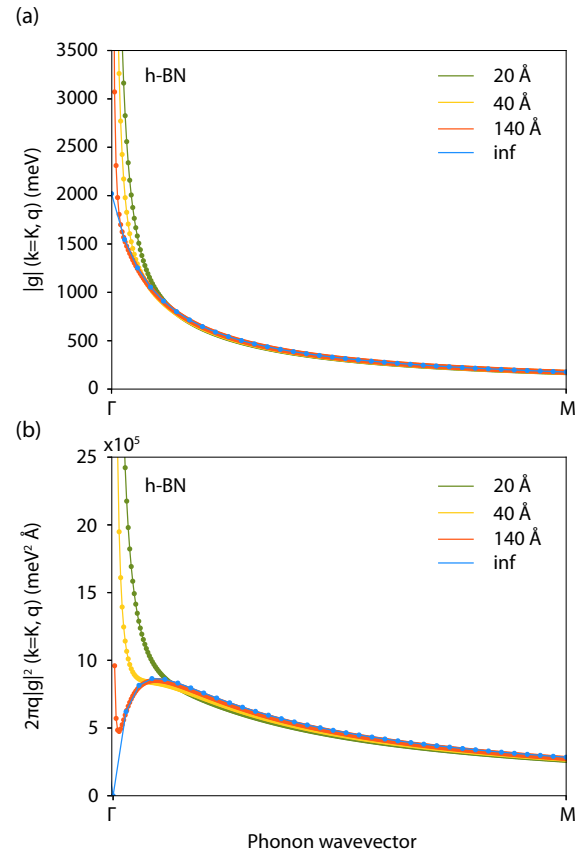

FIG. 6. (a) Modulus of the long-range part of the electron-phonon matrix element, $|g_{mn\nu}(\mathbf{k}, \mathbf{q}_\parallel)|$, for m, n, ν corresponding to the valence band top of h-BN at the K point and the LO mode. We consider phonon wave vectors along the ΓM path. These data were calculated using Eq. (34), for various supercell sizes c along the z direction: $c = 20$ Å(green), 40 Å (yellow), 140 Å (orange), and $c \rightarrow \infty$ (blue). (b) Same raw data as in (a), but this time plotted as $2\pi |\mathbf{q}_\parallel||g_{mn\nu}(\mathbf{k}, \mathbf{q}_\parallel)|^2$.

We can see that, for all finite values of c, the matrix element exhibits a singularity at $\mathbf{q}_\parallel = 0$, as in the case of the 3D Fröhlich interaction. See, for example, the curve for $c = 140$ Å in Fig. 6(a). Although a nonsingular matrix element is only obtained for $c \rightarrow \infty$, calculations using finite supercell sizes are still meaningful, because what matters in actual calculations is the *integral* of the square modulus of the matrix element over the Brillouin zone, as already discussed in relation to Eq. (67). Figure 6(b) shows that this quantity converges to the infinite-vacuum case with increasing c. Correspondingly, the singular region of the Brillouin zone shrinks as c increases, so that the contribution of the singularity to Eq. (67) tends to become negligible at large c. Therefore, supercell calculations *without* Coulomb truncation constitute a viable strategy for studying Fröhlich interactions in 2D and quasi-2D systems, with the proviso that the Wannier-Fourier interpolation strategy of Ref. [32] be *replaced* by the generalized interpolation procedure given by Eq. (34), and that the convergence of the target physical property with respected to supercell size c be achieved.

One further option that could be explored to accelerate the convergence of the calculations, is to combine our matrix

elements at finite c with our expressions for $c \to \infty$. For example, if we call g^{DFPT} the matrix element obtained by direct DFPT calculations on a coarse Brillouin-zone grid, $g^{\text{2D}}(c)$ the matrix element obtained from Eq. (34) with a finite supercell size c, an $g^{\text{2D}}(c = \infty)$ the matrix element obtained from the limit form in Eq. (51), we could envision a Wannier-Fourier interpolation strategy as follows: (1) Perform supercell calculations without Coulomb truncation, yielding g^{DFPT}. (2) Remove the long-range component by subtracting $g^{\text{2D}}(c)$. This defines the short-range component $g^{\text{sr}} = g^{\text{DFPT}} - g^{\text{2D}}(c)$. (3) Interpolate the short-range component as usual [35]. (4) Add to the interpolated short-range matrix elements the long-range component corresponding to the infinite-supercell limit, $g = g^{\text{sr}} + g^{\text{2D}}(c = \infty)$. This approach could also serve to test the convergence of the calculations on the coarse grid vs supercell size c.

VII. CONCLUSION

In this work we developed a unified description of the *ab initio* Fröhlich matrix element that enables calculations of long-range polar electron-phonon couplings in 3D and 2D materials within a single formalism. We showed that the present approach recovers the limits of bulk 3D materials and isolated 2D materials obtained in previous literature. In particular, our generalized matrix element reduces to the 3D Fröhlich matrix element of Ref. [32] when the interlayer separation D between periodic images of the slab vanishes, and it reduces to the 2D Fröhlich matrix element of Ref. [26] when the interlayer separation D becomes infinite.

We validated our methodology by performing DFPT calculations for two systems, monolayer h-BN and monolayer MoS$_2$. In each case, we performed DFPT calculations using finite-size supercells without Coulomb truncation, as well as DFPT calculations employing 2D Couloumb truncation. In both cases our Fröhlich matrix element successfully matches explicit DFPT calculations in the long-wavelength region. These results indicate that the present technique is ready to be employed in conjunction with Wannier-Fourier interpolation of the electron-phonon matrix element [35]. In particular, the present approach can be implemented as a straightforward extension of the method of Ref. [32] in existing software packages like EPW [77].

In this work we also developed a minimal model of polar electron-phonon interactions in 2D. In fact, Eq. (62) provides a simple yet very accurate expression for the Fröhlich matrix

element that depends on only the lattice parameters, the characteristic phonon energy, and the static and high-frequency dielectric constants of the 2D material. Although similar expressions were reported in previous literature [26,27], this work establishes a transparent and direct link with macroscopic materials properties that are readily available. We expect that this minimal model will facilitate the investigation of Fröhlich couplings in 2D using model Hamiltonian approaches, and will help extracting the essential physics from advanced *ab initio* calculations.

We hope that the present cross-dimensional generalization of the *ab initio* Fröhlich matrix element will enable further work in the physics of electron-phonon interactions in semiconductor/insulator interfaces, surfaces, 2D materials and their heterostructures.

APPENDIX: KERNEL FUNCTION

In this Appendix we provide the complete expression for the the kernel function $K(\mathbf{Q}, \tau_z)$ introduced in Eq. (28) and used in the generalized Fröhlich matrix element in Eq. (34):

$$
\begin{aligned}
K(\mathbf{Q}, \tau_z) = {} & \frac{1}{\gamma^- - \gamma^+} \frac{1}{Q^2} \Big\{ [(\alpha + \gamma^- \beta)e^{Q_\| \tau_z} + (\beta + \gamma^- \alpha)e^{-Q_\| \tau_z}] \\
& \times \Big[(\alpha + \gamma^+ \beta)(e^{(Q_\| - iQ_z)\tau_z} - e^{-(Q_\| - iQ_z)d})(Q_\| + iQ_z) - (\beta + \gamma^+ \alpha)(e^{-(Q_\| + iQ_z)\tau_z} - e^{(Q_\| + iQ_z)d})(Q_\| - iQ_z) \\
& + \frac{\alpha + \gamma^+ \beta}{e^{-iQ_z c + \eta} - 1}(1 - e^{-(Q_\| - iQ_z)d})(Q_\| + iQ_z) - \frac{\beta + \gamma^+ \alpha}{e^{-iQ_z c + \eta} - 1}(1 - e^{(Q_\| + iQ_z)d})(Q_\| - iQ_z) \\
& + \frac{1}{e^{-iQ_z c + \eta} - 1}(e^{(Q_\| - iQ_z)D} - 1)(Q_\| + iQ_z) - \frac{\gamma^+}{e^{-iQ_z c + \eta} - 1}(e^{-(Q_\| + iQ_z)D} - 1)(Q_\| - iQ_z) \Big] \\
& + [(\alpha + \gamma^+ \beta)e^{Q_\| \tau_z} + (\beta + \gamma^+ \alpha)e^{-Q_\| \tau_z}]
\end{aligned}
$$

$$\times \left[(\alpha + \gamma^- \beta)(1 - e^{(Q_\parallel - iQ_z)\tau_z})(Q_\parallel + iQ_z) - (\beta + \gamma^- \alpha)(1 - e^{-(Q_\parallel + iQ_z)\tau_z})(Q_\parallel - iQ_z) \right.$$

$$+ \frac{\alpha + \gamma^- \beta}{e^{iQ_z c + \eta} - 1}(1 - e^{-(Q_\parallel - iQ_z)d})(Q_\parallel + iQ_z) - \frac{\beta + \gamma^- \alpha}{e^{iQ_z c + \eta} - 1}(1 - e^{(Q_\parallel + iQ_z)d})(Q_\parallel - iQ_z)$$

$$+ (e^{(Q_\parallel - iQ_z)D} - 1)(Q_\parallel + iQ_z) - \gamma^-(e^{-(Q_\parallel + iQ_z)D} - 1)(Q_\parallel - iQ_z)$$

$$\left. + \frac{1}{e^{iQ_z c + \eta} - 1}(e^{(Q_\parallel - iQ_z)D} - 1)(Q_\parallel + iQ_z) - \frac{\gamma^-}{e^{iQ_z c + \eta} - 1}(e^{-(Q_\parallel + iQ_z)D} - 1)(Q_\parallel - iQ_z) \right] \right\}. \tag{A1}$$

The definitions of the parameters α, β, $\gamma^\pm$, and η are given in Eqs. (20)–(23).

[1] F. Giustino, Rev. Mod. Phys. **89**, 015003 (2017).

[2] A. A. Balandin and D. L. Nika, Mater. Today **15**, 266 (2012).

[3] S. Ishiwata, Y. Shiomi, J. Lee, M. Bahramy, T. Suzuki, M. Uchida, R. Arita, Y. Taguchi, and Y. Tokura, Nat. Mater. **12**, 512 (2013).

[4] J. Noffsinger, E. Kioupakis, C. G. Van de Walle, S. G. Louie, and M. L. Cohen, Phys. Rev. Lett. **108**, 167402 (2012).

[5] M. Zacharias, C. E. Patrick, and F. Giustino, Phys. Rev. Lett. **115**, 177401 (2015).

[6] D. Novko and M. Kralj, NPJ 2D Mater. Appl. **3**, 48 (2019).

[7] G. Eliel, M. Moutinho, A. Gadelha, A. Righi, L. Campos, H. Ribeiro, P.-W. Chiu, K. Watanabe, T. Taniguchi, P. Puech *et al.*, Nat. Commun. **9**, 1221 (2018).

[8] B. Miller, J. Lindlau, M. Bommert, A. Neumann, H. Yamaguchi, A. Holleitner, A. Högele, and U. Wurstbauer, Nat. Commun. **10**, 1 (2019).

[9] X. Cong, X.-L. Liu, M.-L. Lin, and P.-H. Tan, NPJ 2D Mater. Appl. **4**, 13 (2020).

[10] J. T. Devreese and A. S. Alexandrov, Rep. Prog. Phys. **72**, 066501 (2009).

[11] C. Verdi, F. Caruso, and F. Giustino, Nat. Commun. **8**, 15769 (2017).

[12] W. H. Sio, C. Verdi, S. Poncé, and F. Giustino, Phys. Rev. Lett. **122**, 246403 (2019).

[13] M.-A. Husanu, L. Vistoli, C. Verdi, A. Sander, V. Garcia, J. Rault, F. Bisti, L. L. Lev, T. Schmitt, F. Giustino *et al.*, Commun. Phys. **3**, 62 (2020).

[14] L. N. Oliveira, E. K. U. Gross, and W. Kohn, Phys. Rev. Lett. **60**, 2430 (1988).

[15] E. Margine, H. Lambert, and F. Giustino, Sci. Rep. **6**, 21414 (2016).

[16] C. E. P. Villegas, A. R. Rocha, and A. Marini, Phys. Rev. B **94**, 134306 (2016).

[17] D. Fan, H. Liu, L. Cheng, J. Liang, and P. Jiang, J. Mater. Chem. A **6**, 12125 (2018).

[18] Y. Kang, H. Peelaers, and C. G. Van de Walle, Phys. Rev. B **100**, 121113(R) (2019).

[19] N. F. Hinsche and K. S. Thygesen, 2D Mater. **5**, 015009 (2017).

[20] S. Poncé, D. Jena, and F. Giustino, Phys. Rev. B **100**, 085204 (2019).

[21] S. Poncé, W. Li, S. Reichardt, and F. Giustino, Rep. Prog. Phys. **83**, 036501 (2020).

[22] S. Poncé and F. Giustino, Phys. Rev. Research **2**, 033102 (2020).

[23] A. K. Geim, Rev. Mod. Phys. **83**, 851 (2011).

[24] K. Andersen, S. Latini, and K. S. Thygesen, Nano Lett. **15**, 4616 (2015).

[25] N. Mounet, M. Gibertini, P. Schwaller, D. Campi, A. Merkys, A. Marrazzo, T. Sohier, I. E. Castelli, A. Cepellotti, G. Pizzi *et al.*, Nat. Nanotechnol. **13**, 246 (2018).

[26] T. Sohier, M. Calandra, and F. Mauri, Phys. Rev. B **94**, 085415 (2016).

[27] K. Kaasbjerg, K. S. Thygesen, and K. W. Jacobsen, Phys. Rev. B **85**, 115317 (2012).

[28] T. Sohier, D. Campi, N. Marzari, and M. Gibertini, Phys. Rev. Materials **2**, 114010 (2018).

[29] T. Deng, G. Wu, W. Shi, Z. M. Wong, J.-S. Wang, and S.-W. Yang, Phys. Rev. B **103**, 075410 (2021).

[30] W. Li, S. Poncé, and F. Giustino, Nano Lett. **19**, 1774 (2019).

[31] H. Fröhlich, H. Pelzer, and S. Zienau, Lond. Edinb. Dubl. Phil. Mag. J. Sci. **41**, 221 (1950).

[32] C. Verdi and F. Giustino, Phys. Rev. Lett. **115**, 176401 (2015).

[33] J. Sjakste, N. Vast, M. Calandra, and F. Mauri, Phys. Rev. B **92**, 054307 (2015).

[34] P. Vogl, Phys. Rev. B **13**, 694 (1976).

[35] F. Giustino, M. L. Cohen, and S. G. Louie, Phys. Rev. B **76**, 165108 (2007).

[36] N. Marzari, A. A. Mostofi, J. R. Yates, I. Souza, and D. Vanderbilt, Rev. Mod. Phys. **84**, 1419 (2012).

[37] J. Ma, D. Xu, R. Hu, and X. Luo, J. Appl. Phys. **128**, 035107 (2020).

[38] R. Bistritzer and A. H. MacDonald, Proc. Natl. Acad. Sci. USA **108**, 12233 (2011).

[39] Y. Cao, V. Fatemi, S. Fang, K. Watanabe, T. Taniguchi, E. Kaxiras, and P. Jarillo-Herrero, Nature (London) **556**, 43 (2018).

[40] P.-Y. Chen, X.-Q. Zhang, Y.-Y. Lai, E.-C. Lin, C.-A. Chen, S.-Y. Guan, J.-J. Chen, Z.-H. Yang, Y.-W. Tseng, S. Gwo *et al.*, Adv. Mater. **31**, 1901077 (2019).

[41] L. J. McGilly, A. Kerelsky, N. R. Finney, K. Shapovalov, E.-M. Shih, A. Ghiotto, Y. Zeng, S. L. Moore, W. Wu, Y. Bai *et al.*, Nat. Nanotechnol. **15**, 580 (2020).

[42] S. D. Sarma and B. Mason, Ann. Phys. **163**, 78 (1985).

[43] F. M. Peeters, W. Xiaoguang, and J. T. Devreese, Phys. Rev. B **33**, 3926 (1986).

[44] J. Sak, Phys. Rev. B **6**, 3981 (1972).

[45] B. A. Mason and S. Das Sarma, Phys. Rev. B **33**, 8379 (1986).

[46] R. Jalabert and S. Das Sarma, Phys. Rev. B **40**, 9723 (1989).

[47] S. Das Sarma, J. K. Jain, and R. Jalabert, Phys. Rev. B **41**, 3561 (1990).

[48] T. Hahn, S. Klimin, J. Tempere, J. T. Devreese, and C. Franchini, Phys. Rev. B **97**, 134305 (2018).

[49] N. Mori and T. Ando, Phys. Rev. B **40**, 6175 (1989).

[50] S. Baroni, S. de Gironcoli, A. Dal Corso, and P. Giannozzi, Rev. Mod. Phys. **73**, 515 (2001).

[51] M. T. Yin and M. L. Cohen, Phys. Rev. B **26**, 3259 (1982).

[52] G. Brunin, H. P. C. Miranda, M. Giantomassi, M. Royo, M. Stengel, M. J. Verstraete, X. Gonze, G.-M. Rignanese, and G. Hautier, Phys. Rev. Lett. **125**, 136601 (2020).

[53] G. Brunin, H. P. C. Miranda, M. Giantomassi, M. Royo, M. Stengel, M. J. Verstraete, X. Gonze, G.-M. Rignanese, and G. Hautier, Phys. Rev. B **102**, 094308 (2020).

[54] J. Park, J.-J. Zhou, V. A. Jhalani, C. E. Dreyer, and M. Bernardi, Phys. Rev. B **102**, 125203 (2020).

[55] V. A. Jhalani, J.-J. Zhou, J. Park, C. E. Dreyer, and M. Bernardi, Phys. Rev. Lett. **125**, 136602 (2020).

[56] F. Giustino, Rev. Mod. Phys. **91**, 019901(E) (2019).

[57] X. Gonze and C. Lee, Phys. Rev. B **55**, 10355 (1997).

[58] A. Ercelebi and G. Süalp, J. Phys. Chem. Solids **48**, 739 (1987).

[59] J. T. Titantah, C. Pierleoni, and S. Ciuchi, Phys. Rev. Lett. **87**, 206406 (2001).

[60] H. Rücker, E. Molinari, and P. Lugli, Phys. Rev. B **45**, 6747 (1992).

[61] L. Cheng and Y. Liu, J. Am. Chem. Soc. **140**, 17895 (2018).

[62] M. Royo and M. Stengel, Phys. Rev. X **11**, 041027 (2021).

[63] F. Giustino and A. Pasquarello, Phys. Rev. B **71**, 144104 (2005).

[64] R. Guseinov, Phys. Status Solidi **125**, 237 (1984).

[65] F. Giustino and A. Pasquarello, Phys. Rev. Lett. **95**, 187402 (2005).

[66] T. Sohier, M. Gibertini, M. Calandra, F. Mauri, and N. Marzari, Nano Lett. **17**, 3758 (2017).

[67] P. Giannozzi, S. Baroni, N. Bonini, M. Calandra, R. Car, C. Cavazzoni, D. Ceresoli, G. L. Chiarotti, M. Cococcioni, I. Dabo, A. D. Corso, S. de Gironcoli, S. Fabris, G. Fratesi, R. Gebauer, U. Gerstmann, C. Gougoussis, A. Kokalj, M. Lazzeri,

L. Martin-Samos *et al.*, J. Phys.: Condens. Matter **21**, 395502 (2009).

[68] P. Giannozzi, O. Andreussi, T. Brumme, O. Bunau, M. B. Nardelli, M. Calandra, R. Car, C. Cavazzoni, D. Ceresoli, M. Cococcioni, N. Colonna, I. Carnimeo, A. D. Corso, S. de Gironcoli, P. Delugas, R. A. DiStasio, A. Ferretti, A. Floris, G. Fratesi, G. Fugallo *et al.*, J. Phys.: Condens. Matter **29**, 465901 (2017).

[69] D. R. Hamann, Phys. Rev. B **88**, 085117 (2013).

[70] M. Schlipf and F. Gygi, Comput. Phys. Commun. **196**, 36 (2015).

[71] J. P. Perdew, K. Burke, and M. Ernzerhof, Phys. Rev. Lett. **77**, 3865 (1996).

[72] D. M. Ceperley and B. J. Alder, Phys. Rev. Lett. **45**, 566 (1980).

[73] J. P. Perdew and A. Zunger, Phys. Rev. B **23**, 5048 (1981).

[74] A. V. Lebedev, I. V. Lebedeva, A. A. Knizhnik, and A. M. Popov, RSC Adv. **6**, 6423 (2016).

[75] T. Sohier, M. Calandra, and F. Mauri, Phys. Rev. B **96**, 075448 (2017).

[76] A. A. Mostofi, J. R. Yates, G. Pizzi, Y.-S. Lee, I. Souza, D. Vanderbilt, and N. Marzari, Comput. Phys. Commun. **185**, 2309 (2014).

[77] S. Poncé, E. Margine, C. Verdi, and F. Giustino, Comput. Phys. Commun. **209**, 116 (2016).

[78] A. Kormányos, G. Burkard, M. Gmitra, J. Fabian, V. Zólyomi, N. D. Drummond, and V. Fal'ko, 2D Mater. **2**, 022001 (2015).

[79] F. Ferreira, A. Chaves, N. Peres, and R. Ribeiro, J. Opt. Soc. Am. B **36**, 674 (2019).

[80] C. Freysoldt, P. Eggert, P. Rinke, A. Schindlmayr, and M. Scheffler, Phys. Rev. B **77**, 235428 (2008).

[81] A. Laturia, M. L. Van de Put, and W. G. Vandenberghe, NPJ 2D Mater. Appl. **2**, 6 (2018).

[82] T. A. C. C. Staff, Texas Advanced Computing Center, Lonestar User Guide, tacc.utexas.edu/user-services/user-guides/lonestar-user-guide.